PARTICLE ADHESION: APPLICATIONS AND ADVANCES

Edited by
David J. Quesnel
Donald S. Rimai
and
Louis H. Sharpe

USA Publishing Office: TAYLOR & FRANCIS
29 West 35th Street
New York, NY 10001
Tel: (212) 216-7800
Fax: (212) 564-7854

Distribution Center: TAYLOR & FRANCIS
7625 Empire Drive
Florence, KY 41042
Tel: 1-800-634-7064
Fax: 1-800-248-4724

UK TAYLOR & FRANCIS
27 Church Road
Hove
E. Sussex, BN3 2FA
Tel.: +44 (0) 1273 207411
Fax: +44 (0) 1273 205612

PARTICLE ADHESION: APPLICATIONS AND ADVANCES

1 2 3 4 5 6 7 8 9 0

Printed by Edwards Brothers, Lillington, NC, 2001.
Cover photo: Figure 6B, page 330 of the article "Interactions Between Micron-sized Glass Particles and poly(dimethyl siloxane) in the Absence and Presence of Applied Load", by Toikka et al.
The articles appearing in this book were originally published in Volume 74, Numbers 1-4 of *The Journal of Adhesion*.

A CIP catalog record for this book is available from the British Library.
The paper in this publication meets the requirements of the ANSI Standard Z39, 48-1984 (Permanence of Paper).

Library of Congress Cataloging-in-Publication Data

Available from publisher

ISBN 90-5699-725-4 (case)

Experiments and Engineering Models of Microparticle Impact and Deposition

RAYMOND M. BRACH, PATRICK F. DUNN and XINYU LI

Particle Dynamics Laboratory, Department of Aerospace and Mechanical Engineering, University of Notre Dame, Notre Dame, IN 46556, USA

This article summarizes, reviews and consolidates some of the research work done by the authors over recent years. It covers a wide variety of topics related to the experimental and analytical investigations of the impact of microparticles with flat surfaces in the presence of adhesion and frictional forces. Over 180 experiments were conducted under vacuum conditions to study the effects of particle size, shape, incident translational and rotational velocities, and substrate surface roughness on the oblique impact response of the particle. Analytical models of the impact process were developed, including an algebraic, rigid-body model and a numerical simulation that can be used to predict rebound and capture conditions and to model the forces and displacements that occur during the contact duration. These models were validated using experimental results. Overall, the article covers impact conditions ranging from the more idealized case of a microsphere impacting a molecularly-smooth surface to the more realistic and complex situation of a biological microparticle impacting a typical indoor-room surface.

1. INTRODUCTION

The following article is a summary of combined experimental and analytical work done in order to study and model the process of impact of microparticles. It begins with a discussion of some of the classical

experimental results already published in the literature. Then, it displays and examines more recent experimental results of the oblique impact of microspheres against ultrasmooth and rough surfaces. Data from the impact of nonsmooth particles (bioaerosols) are also presented.

Two analytical models of the planar oblique impact process in the presence of adhesion are summarized and discussed. One is an algebraic model based on rigid body[1] impact theory and which uses coefficients to represent the impact process. Another is based on the Hertzian elastic model in the contact region but which also takes into account an adhesion force as well as distinct representation of material and adhesion dissipation. The latter model, referred to as a dynamic simulation, is based directly on Newton's differential equations of motion and its solution is through numerical integration.

In addition to the impact models, another model is developed. It is a set of empirical equations that represent the kinematic coefficient of restitution of the rigid body model as a function of initial normal velocity. These equations when combined with the rigid body equations allow specific behavior, including capture, to be modeled for applications.

Finally, several analyses are carried out that relate to the impact process of microspheres. One studies the influence of surface roughness on the measured values of the coefficient of restitution and the frictional, coefficient for oblique collisions. The analysis shows that small unknown variations in the slope of the surface can lead to biased coefficient values computed from experimental measurements. A second analysis uses the rigid body impact model with Monte Carlo methods to investigate both the effects of surface roughness and the impact process. A third analysis is a sensitivity study of the different factors such as physical constants of the impact process and shows which are the most significant in controlling capture of a particle due to adhesion.

2. EXPERIMENTS ON MICROPARTICLE IMPACT

Many definitive experimental studies of microparticle impact onto surfaces exist, including the pioneering work of Dahneke [1], as well as

[1]The term *rigid body* here denotes the presence of rotational inertia (in contrast to a point mass) and does not imply inflexibility.

the work of Wang *et al.* [2], Wall *et al.* [13] and Dunn *et al.* [4, 5]. Experiments can be categorized into those limited to normal impacts and those including oblique impacts. Both involve the effects of adhesion but only the oblique collisions display effects of friction. The results of the microparticle/substrate surface impact experiments of Dunn *et al.* [4, 5] and Li *et al.* [5] are summarized in this section. In all, 187 different experimental combinations were conducted that included metal and glass microspheres and lycopodium spores, 5 different ranges of microsphere diameters, 11 different surface types, 14 different surface angles and about 14 different ranges of initial microparticle velocities. Each experiment consisted of approximately 40 individual impact events. All experiments were conducted under vacuum and neutral charge conditions in order to obviate the effects of additional forces acting near or during surface contact. The approach taken was first to investigate the most idealized impact conditions of microsphere impact with a molecularly-smooth, planar surface. Then, additional factors such as a wider particle-size distribution, a rougher substrate surface and a more complex particle surface were introduced in steps in order to understand each of their effects on impact and capture.

2.1. Equipment and Methods

This section describes the basic experimental facility used for the experiments, which was developed by Caylor [6] and described in detail by Dunn *et al.* [4]. The physical attributes of the microparticles and surfaces are described later when the results are presented. The system primarily consisted of a vacuum test cell (at 10^{-4} Torr), particle dispenser and target surface. In these experiments, the microparticles were dispensed using a neutral-charge particle dispenser (NPD) and in all cases the target surface was electrically grounded. The microparticles were placed on the bottom dispenser plate of the NPD. A rotor underneath the plate periodically contacted the plate and vibrated it, causing the microspheres to fall through a hole at its center. To control the falling particles, a hypodermic needle was connected to the hole. As a result, the microspheres were directed downward in a straight trajectory to the target surface. Once a particle was ejected from the NPD, it was accelerated by gravity to the target surface. The vertical distance between the dispenser and the target

surface varied from 0.01 m to 1.0 m, providing a velocity range from 0.44 m/s to 4.4 m/s.

For oblique impact experiments in which the target surface was inclined at an angle with respect to the incident particle beam, a particle trajectory imaging system (PTIS) was used to record the microparticles incident and rebound trajectories, from which the velocity components were determined. This set-up is shown in Figure 1. The PTIS was comprised of an argon-ion laser, beam chopper, plano-convex lens, CCD camera and video recorder. The PTIS generated a pulsed laser light sheet that illuminated the individual particle as it approached and rebounded from the surface. The trajectories were processed to obtain the particle's incident and rebound angles and speeds. For this PTIS setup, an argon-ion laser beam (operated nominally at 1W) passed through a collimator to control the beam width to provide as narrow a light sheet as possible. The laser beam was then directed through a spinning disk with 10 evenly-spaced slots to produce a pulsed laser beam. Depending on the

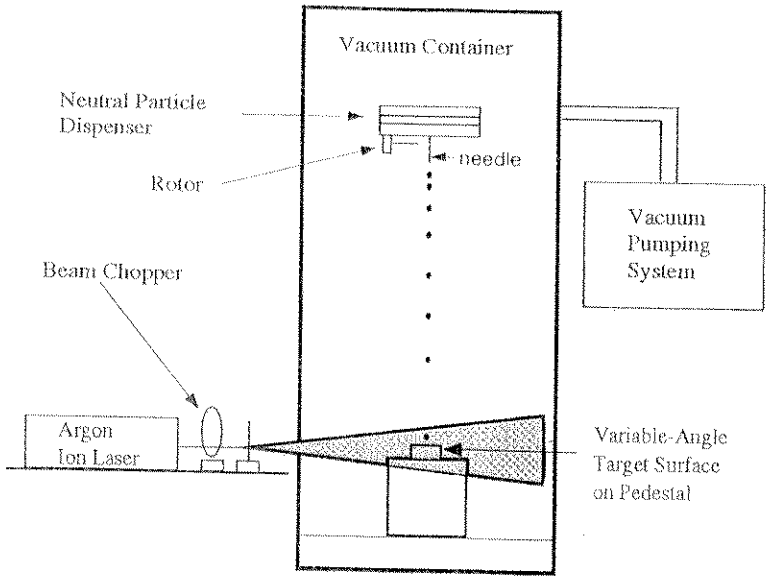

FIGURE 1 Schematic layout of the experimental equipment used for oblique impact experiments.

angular velocity of the disk, the pulsed frequency could be varied to obtain the desired track length. The chopped beam then passed through a plano-convex lens that formed a pulsed light sheet aligned in a vertical plane above the target surface. In preparing an experiment, another laser beam was sent through the hypodermic needle to make sure this laser beam was at the center of the pulsed light sheet. Video data were taken through a porthole located at the side of the vacuum chamber using a CCD camera and a video cassette recorder. The camera was installed approximately 90° to the light sheet. The image was enlarged as much as possible to get a clear trajectory. Based on the frame rate, the field of view, and the strobe frequency, the system could measure particle velocities ranging from about 0.1 to 30 m/s.

For normal impact experiments using microspheres, a two-dimensional phase Doppler particle analyzer (PDPA) was used in the 90° side-scatter mode to determine each microsphere's incident and rebound vertical velocity components and its diameter. The top view of this set-up is shown in Figure 2. The probe volume was positioned about 1 mm above the surface. Frequency shifting was used to discriminate between the incoming and outgoing particles. The particle size was determined from the Doppler signal based on the phase

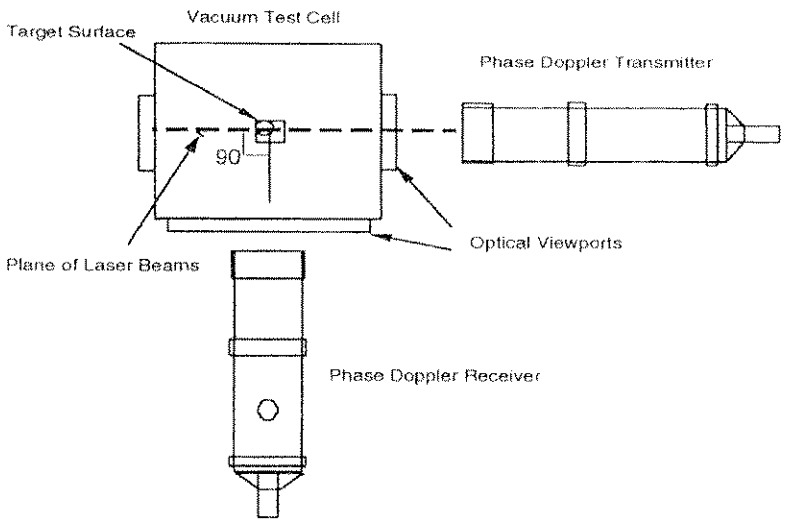

FIGURE 2 Top view of experimental set-up used for normal impact experiments.

differences between the three detectors. The system's laser was an air-cooled argon ion laser; the output power could be varied from 20 to 300 mW to obtain satisfactory scattered light intensity over the wavelength range between 454 and 514 nm. The raw PDPA data (including the incident and rebound velocity component values, particle diameter and time of acquisition) was stored in a data file. After the experiment, the data were processed to identify the incident and rebound normal velocity components for the *same* microsphere. This was accomplished by using an initial estimate of the vertical distance, h, between the laser probe volume and the target surface to initiate a pair-searching algorithm. Separate experiments were conducted to verify that the distance between the laser probe volume and the surface had no effect on pair identification. Finally, the paired velocity data corresponding to the position of laser probe volume were corrected by $\pm\sqrt{2gh}$ to give the velocity components at the surface. In this manner, the various parameters of interest could be computed for each individual impact event and then, subsequently, averaged over 40 individual events for an experiment.

Details of an uncertainty analysis of the above process can be found in Caylor [6] and in Dunn *et al.* [4]. The measurement and finite sampling uncertainties are combined to provide estimates of the true mean values at 95% confidence for each parameter. In the following presentation of the experimental data, the sample mean value of a quantity is plotted with an error bar. Each data point represents the sample mean value of approximately 40 *individual* impact events. An error bar designates the range within which the true mean value lies with respect to the sample mean value within a 95% probability.

2.2. Experimental Parameters

There are three experimental parameters that are used to characterize the impact event. These are the coefficient of restitution, e, the impulse ratio, μ, and the normalized translational kinetic energy loss, T_L. Referring to Figure 3, these parameters are defined as follows:

$$e = -V_n/v_n \tag{1}$$

$$\mu = (V_t - v_t)/(V_n - v_n) \tag{2}$$

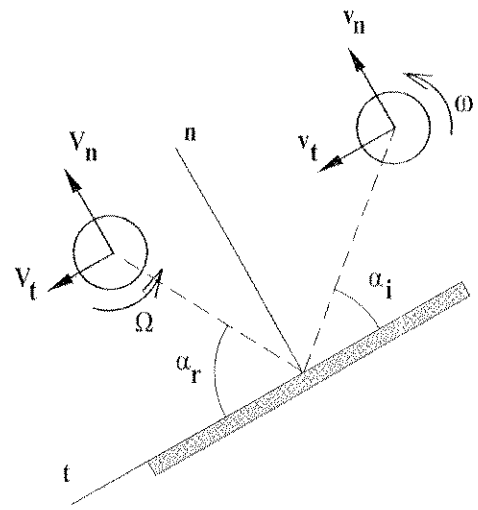

FIGURE 3 Variables and coordinates used for planar impact measurements.

$$T_L = (v^2 - V^2)/v^2 \tag{3}$$

Their derivations and physical interpretations will be presented in the section describing the analytical models. The following experimental results are presented in their context.

2.3. Normal Impact Results

Dahneke [1, 8] studied the capture velocity of 1.27 μm-diameter polystyrene latex spheres. In these experiments, it was found that a particle with an incoming velocity less than a critical velocity would stick to the surface, otherwise, if it had a larger velocity, it would rebound from the target surface. He also suggested that the elastic flattening during contact is very important. Dahneke [8] measured the particle velocity before and after collision directly. The velocity was determined by measuring the time for a particle to pass through two parallel laser beams. Dahneke found that the coefficient of restitution, defined as the ratio of rebound velocity over the incoming velocity, increased with the incoming velocity just above the critical (capture) velocity, reached an asymptotic level for some range of velocities and then finally decreased at higher incoming velocities.

Paw U [9] obtained the speed at impact for normal incidence above which ragweed pollen and lycopodium spores rebound from glass and the leaves of various plants. The results suggested that the geometry and material properties of the particle are more important than those of the surface to determine the critical velocity.

By using a high speed camera system, Rogers and Reed [10] measured the capture velocities for three different kinds of particles (copper, glass, steel) impacting onto surfaces. The results showed that the capture velocity is inversely related to the particle size. Although plastic deformation during contact was a focal point of the study, little or no evidence of plastic deformation was given.

With the help of laser Doppler velocimetry, Wall *et al.* [3] measured the velocities of incoming and rebounding ammonium fluorescein spheres having different diameters (2.58, 3.44, 4.90 and 6.89 μm). The velocity range was from about 1 m/s, near the capture threshold, up to 100 m/s. It was found that capture velocity decreases with a power-law dependence on particle size rather than the elastic flattening model proposed by Dahneke [7]. Plastic deformation was used in this study as the sole mechanism of energy dissipation. Yet, no observable evidence of plastic deformation was cited.

Dunn *et al.* [4] reported the experimental results of both normal and oblique impact of microspheres on different surfaces. A phase Doppler particle analyzer and a particle trajectory imaging system were applied to measure the particle velocity. It was found that, for an incidence velocity larger than 3 m/s, the coefficient of restitution was almost constant. This was consistent with the results of Dahneke [8] and Wall *et al.* [3]. When the velocity was less than 3 m/s, the coefficient of restitution decreased rapidly. Results also showed that the material properties affected the impact process. No capture velocities were obtained from the experiments.

Li *et al.* [5] reported the results of the normal impact of polydisperse stainless steel microspheres with molecularly-smooth silicon surfaces at velocities near the capture velocity. These experimental results were compared with a dynamic simulation model, which was used to predict the capture velocity. The predicted capture velocity was consistent with experimental observations.

In summary, for normal impact, experiments show that the capture velocity is related to the particle size, initial velocity, surface geometry and material properties. Yet, because there are no experiments in which the capture velocity has been measured directly, no direct verification of any theoretical models of the capture velocity has been made.

2.3.1. The Effect of Particle Diameter

Experiments that reveal that the most "classic" results are those involving the impact of microspheres onto a molecularly-smooth substrate surface. One set of experiments in this category used two kinds of Type 316 stainless steel microspheres, each with a different size range (SST65, 10 to 65 μm, $d_{10} = 49$ μm and SST125, 60 to 125 μm, $d_{10} = 75$ μm).[2] The target surface was a molecularly-smooth (to within 5 Angstroms) [1, 0, 0] plane silicon crystal. As shown in Figure 4 (SST65 solid squares; SST125 open squares), both cases display a similar trend; at higher initial velocities (above about 0.75 m/s), the coefficient of restitution is roughly constant. At lower initial velocities, the coefficient of restitution decreases as the initial velocity decreases.

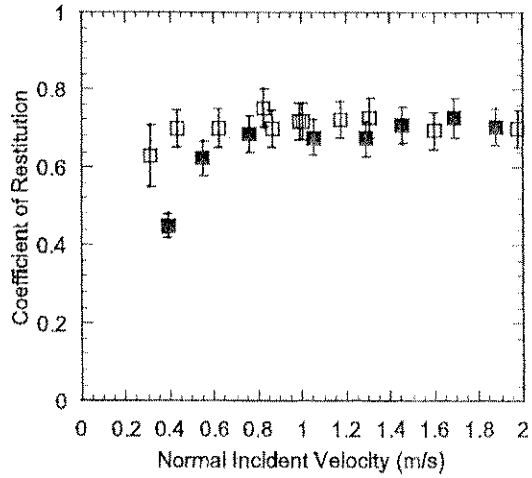

FIGURE 4 Coefficient of restitution from the normal impact of SST microspheres with diameters of $d_{10} = 49$ μm (solid squares) and $d_{10} = 75$ μm (open squares) for a molecularly-smooth, planar silicon crystal surface.

[2] d_{10} is the mean of the distribution of diameter.

This effect is more pronounced for smaller diameter particles indicating that adhesion effects are more significant for smaller diameter particles. Such trends with particle diameter agree with findings of Wall *et al.* [3].

For normal impact, the normal component is the total velocity. Thus, $T_L = 1 - e^2$. The normalized energy loss varying with the normal velocities is shown in Figure 5. It can be seen that, when incoming velocity gets smaller, the normalized kinetic energy loss becomes larger. This implies that, due to the effects of adhesion, there is more energy dissipation of the initial kinetic energy for impacts occurring at lower normal velocities. As a result, the microparticle will be captured if the incoming velocity becomes much smaller. The experiments showed that the microspheres started to pile up on the substrate surface (*i.e.*, were captured by the surface) at about 0.2 to 0.3 m/s. Because of the range of microsphere sizes, it was impossible to measure directly an exact capture velocity from the present experimental setup.

In summary, effects of adhesion manifest themselves at lower incident normal velocities, resulting in a decrease of the coefficient of restitution and an increase in the normalized translational kinetic energy loss. This effect occurs at relatively higher incident normal

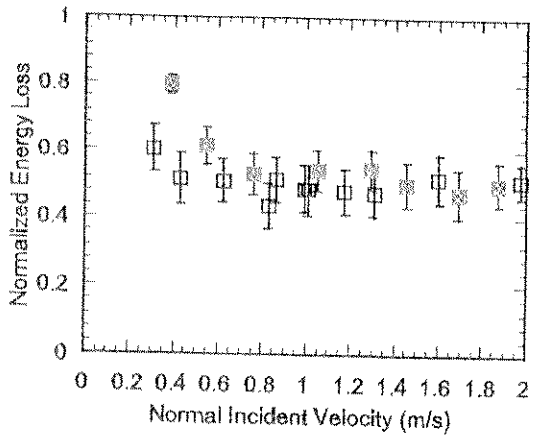

FIGURE 5 Energy loss from the normal impact of SST microspheres with diameters of $d_{10} = 49\,\mu m$ (solid squares) and $d_{10} = 75\,\mu m$ (open squares) for a molecularly-smooth, planar silicon crystal surface.

velocities for smaller diameter microspheres. This inherently leads to a lower capture velocity for larger diameter microspheres.

2.4. Oblique Impact Results

Broom [11] used glass spheres impacting on aluminum to study the adhesion of particles in filters. The nominal impact angles were 90° and 45°. A high speed camera system was used to take pictures of the particle trajectory and, further, to deduce the velocity. The results showed that the capture velocity was smaller for oblique impact, which implied that the particle rebounded more easily from the oblique surface than from the normal surface. It was also found that the nature of the impact surface is important; a polished surface exhibited an efficiency of capture higher than a rough surface.

Aylor and Ferrandino [12] studied the sticking probability of ragweed pollen and lycopodium spores impacting on glass cylinders and wheat stems. It was found that the speed for onset of rebound of a ragweed pollen was about 1.7 times as great as the critical speed for lycopodium spores. Changes in wheat stem characteristics as the plant aged also produced a measurable effect on this sticking efficiency. The experiments showed that the coefficient of restitution might not be constant for all impacts angles, but increases when the angle of impact becomes more oblique.

Wang *et al.* [2] investigated the adhesion efficiency of particles on a cylinder. Their measurements of particle rebound as a function of the position angle on the cylinder showed that rebound increases rapidly with angle. It was suggested that the tangential velocity component caused particle bounce, which possibly occurs through interaction with surface roughness.

Buttle *et al.* [13] conducted experiments with glass spheres impacting onto an aluminum substrate at 90° (normal), 50° and 29° respectively. The velocity was measured using laser Doppler velocimetry. The value of coefficient of restitution increased from around 0.5 at normal and 50° impact to 0.68 at 29° impact. This was considered to be the result of frictional force reduction and rotation of particle at very oblique impact.

Using the particle image technique, Dunn *et al.* [5] studied the effects of impact caused by the surface material properties and roughness,

microsphere spin, particle size and electrical charge. It was found that surface roughness significantly biased the experimental results for very shallow (glancing) angles of incidence, yielding an unrealistically high value for the coefficient of restitution. Through examination of the microsphere's impulse ratio, four regions of different surface contact mechanics can be identified (in order of decreasing incident angle): a "rolling region" in which the microspheres are rolling without sliding by the end of contact, a "transition region" in which some of the microspheres slide throughout contact and some end up only rolling, a "sliding region" in which the microspheres all are sliding at the end of contact and the impulse ratio value is constant and, lastly, a region characterized by changes from a constant impulse ratio value. The initial spin of the particle also increased the uncertainty of the impulse ratio for a particular incidence angle.

In summary, the results of oblique impact experiments suggest that the capture velocity will not be a constant for all the impacting angles; the more oblique the impact angle, the smaller the capture velocity. The introduction of a friction force in addition to an adhesion force clearly makes the impact process more complex. Most of the data were acquired with the target surfaces oriented at various angles with respect to the incident particle trajectory. The cases examined ranged from the more idealized case of a microsphere impacting a molecularly-smooth surface to the more realistic and complex situation of a biological microparticle impacting a typical indoor-room surface. In the following, the oblique impact results are presented in the context of illustrating the effects of various parameters on the impact process.

2.4.1. The Effect of Surface Roughness

One of the first questions to be addressed is how the roughness of the substrate surface affects the microparticle's impact response. This is examined experimentally through comparison of various cases of "rough" substrate surfaces with that of the molecularly-smooth substrate surface. A base case for comparison is chosen as a relatively-monodisperse stainless steel microsphere (SST76, $d_{10} \approx 62\,\mu\text{m}$) impacting a molecularly-smooth substrate surface ([1, 0, 0] plane silicon crystal).

The results of the base case for a nominal incident normal velocity of 1.66 m/s are shown in Figure 6, in which the solid symbols denote the smooth-surface base case and the open symbols the "rough"

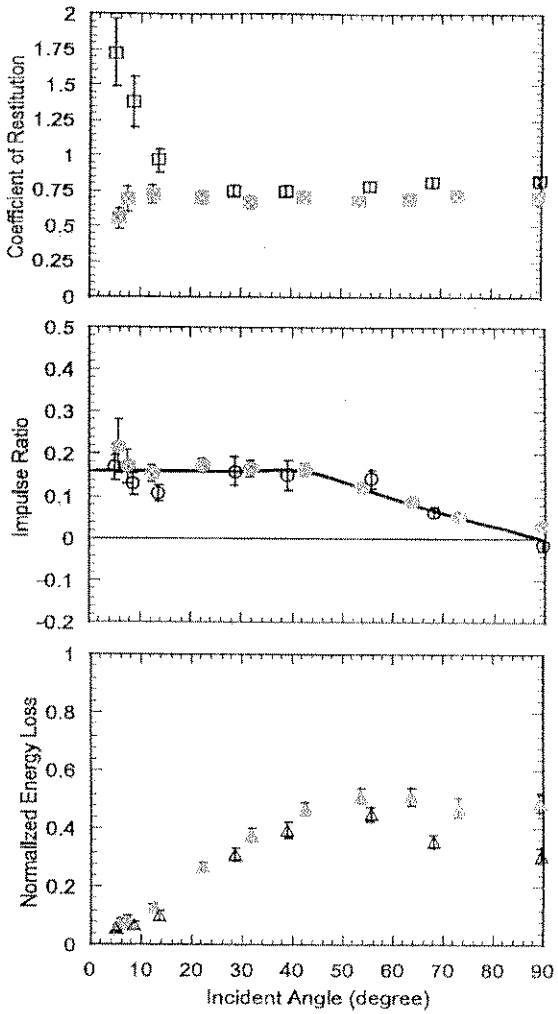

FIGURE 6 Comparisons of e, μ and T_L for a nominal incident normal velocity of 1.66 m/s where the solid symbols are from the smooth-surface (molecularly-smooth, planar silicon crystal) and the open symbols the "rough" surface case (back side of the same silicon surface). The solid curve is for the impulse ratio under the conditions of Coulomb friction and no initial angular velocity.

surface case. As shown in the figure, the coefficient of restitution is relatively constant ($e \approx 0.70$) with incident angle, except at incident angles of approximately 10° or less, where it decreases to $e \approx 0.50$. The impulse ratio curve exhibits a classic rolling-throughout-contact-duration behavior [15] from 90° down to approximately 50°, where it transitions to a constant value of $\mu \approx 0.15$. It is presumed that this value corresponds to that of the coefficient of friction between stainless steel and silicon. Below approximately 15°, the impulse ratio rises slightly. (The reason for this will be discussed in the section on analytical models.) The normalized translational kinetic energy loss is maximum at the higher incident angles, where most of the loss occurs due to overcoming surface adhesion.

The comparative rough substrate case consists of the same particles and the "rough" back-side of a silicon crystal. The results in Figure 6 are denoted by the open squares. It is seen that for incident angles larger than 20° the coefficient of restitution for the rough surface was slightly larger than that of the smooth surface. At lower incident angles (less than about 20°), values of the coefficient for the rough surface were much higher than those for the smooth surface. In fact, coefficient of restitution values exceed unity, which is not physically possible. Because of surface roughness, the "true" surface normal direction differs from the "nominal" normal and biases the value of e calculated using the nominal normal velocity components.[3] This is explained in detail later in Section 4. As far as the impulse ratio is concerned, for the rough surface the impulse ratio was not higher than that of the smooth surface, which implied that the rough surface might not result in a larger friction coefficient as expected. Because the adhesion force may contribute to the friction, if the adhesion force was smaller for rough surface, the friction may be smaller for the rough surface also. The normalized energy loss was less for the rough surface when the incident angles were higher than 50°, which might indicate that adhesion dissipation is less significant for rough surface impact. Whether or not the adhesion dissipation force could cause such an obvious influence on the normalized energy loss is still open to question.

[3]This is analogous to viewing the surface of the earth as flat when modeling meteorite impacts. On a broad plain or plateau the normal direction is close to a radial line but in a mountainous region the actual normal can differ greatly.

Additional cases were run to compare smooth with rough surface impact behavior. Shown in Figure 7 are the results of another comparison, in which the smooth surface is a "first-surface" mirror and

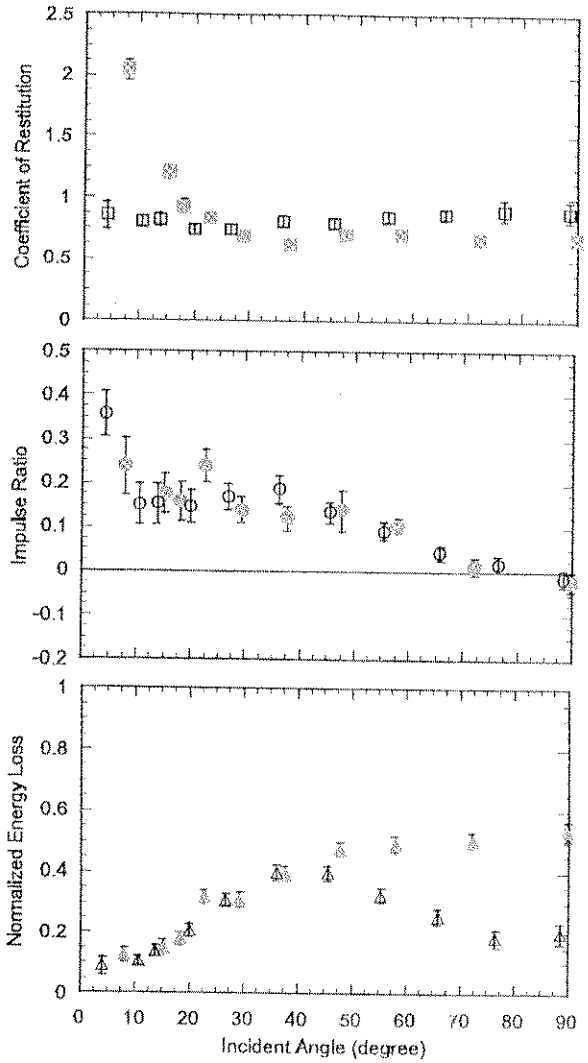

FIGURE 7 Comparisons of e, μ and T_L for a nominal incident normal velocity of 1.66 m/s where the solid symbols are from the smooth-surface (a "first-surface" mirror) and the open symbols the "rough" surface case (back side of the mirror).

the rough surface is the back-side of the same material. The comparison reveals some similar trends and some differences from what was previously observed. The coefficient of restitution values here are higher than before ($e \approx 0.70 - 0.90$ *versus* $e \approx 0.70 - 0.75$). Measured values of e for the rough case again increase to beyond unity at the lower incidence angles. The impulse ratio behavior is similar. The normalized translational kinetic energy loss, however, shows the opposite trend for the second rough-*versus*-smooth surface case, in that the rough surface case exhibits higher losses at high incidence angles. This can be explained by noting that this energy loss varies as $(1 - e^2)$ at high incidence angles. Consequently, because e is lower energy loss will be higher.

To summarize, surface roughness can cause the measured value of the coefficient of restitution to be greater than unity at very low incidence angles (see Section 4) and change the amount of translational energy loss at higher incidence angles.

2.4.2. The Effects of Incident Rotational and Translational Velocities

Another consideration in characterizing a microparticle's impact response is to identify how the microparticle's incident rotational and translational velocities influence its capture or rebound. Incident translational velocities are changed easily by varying the spacing between the particle dispenser and the target surface. Rotational velocities, however, cannot be controlled, cannot be measured and possibly can vary systematically from one spacing to another. For this set of experiments, 11 different cases were studied. Relatively monodisperse stainless steel microspheres (SST65) were used along with the molecularly-smooth substrate surface ([1, 0, 0] plane silicon crystal). Results for e, μ and T_1, *versus* incident angle are presented in Figures 8–10, for 3 of the 11 incident velocity cases examined. The incident velocity ranges were from 1.59 to 1.69 m/s for the 1.60 m/s case; from 1.01 to 1.09 m/s for the 1.05 m/s case; and from 0.39 to 0.49 m/s for the 0.45 m/s case. In Figure 8, the coefficient of restitution decreased slightly with the decreasing nominal incident velocity from 1.60 m/s to 0.45 m/s. For the same nominal incident velocity, the coefficient of restitution decreased slightly with decreasing incident

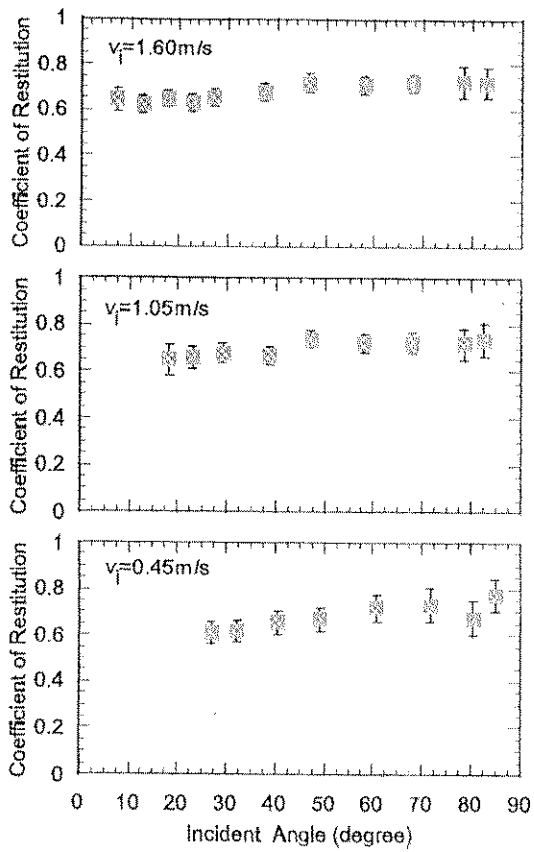

FIGURE 8 Comparisons of the coefficient of restitution, e, for stainless steel microspheres (SST65) with a molecularly-smooth, planar silicon crystal surface for 3 different ranges of total initial velocities; values indicated are nominal values.

angle. For the low incident velocity case ($v = 0.45$ m/s), the decreasing trend was more significant. For the higher incident velocity case ($v = 1.60$ m/s), the decrease in the coefficient of restitution was slight and the trend was not consistent at very shallow incident angles. The average value changed from 0.70 to 0.65 with the incident angle decreasing from 85° to 25°. Because the incident normal velocity decreases with decreasing incident angle (because the total velocity is held constant), the coefficient of restitution consequently decreases with the decreasing of the normal velocity component. For some cases,

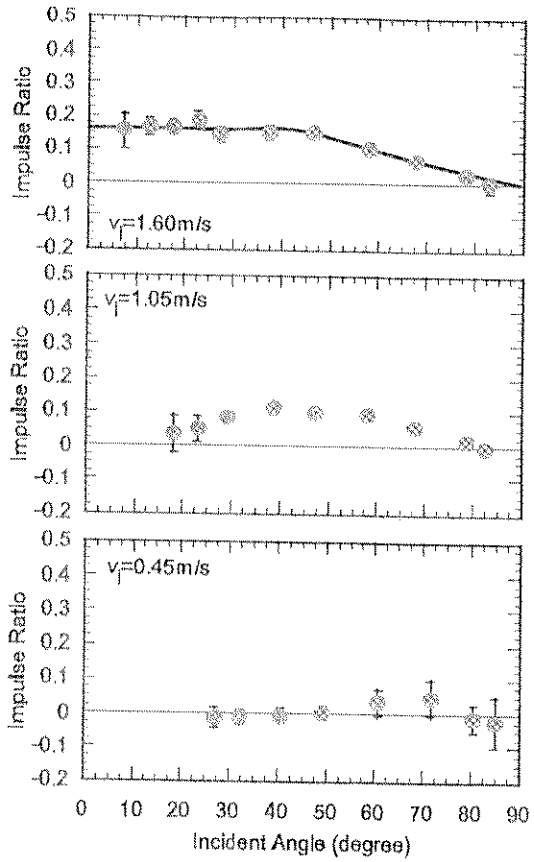

FIGURE 9 Comparisons of the impulse ratio, μ, for stainless steel microspheres (SST65) with a molecularly-smooth, planar silicon crystal surface for 3 different ranges of total initial velocities; values indicated are nominal values. The solid curve is the impulse ratio for coulomd friction from the rigid body model.

the normal velocity component was lower than the capture velocity of normal impact ($\approx 0.2-0.3$ m/s for SST76), yet no capture was observed and the coefficient of restitution was still rather high. This implies that, for oblique impact, the capture velocity is different from that for normal impact.

The impulse ratio behavior is shown in Figure 9. For $v = 1.60$ m/s, in the region of incident angles from 90° to 50°, the impulse ratio increases with decreasing incident angle. This is the "rolling region",

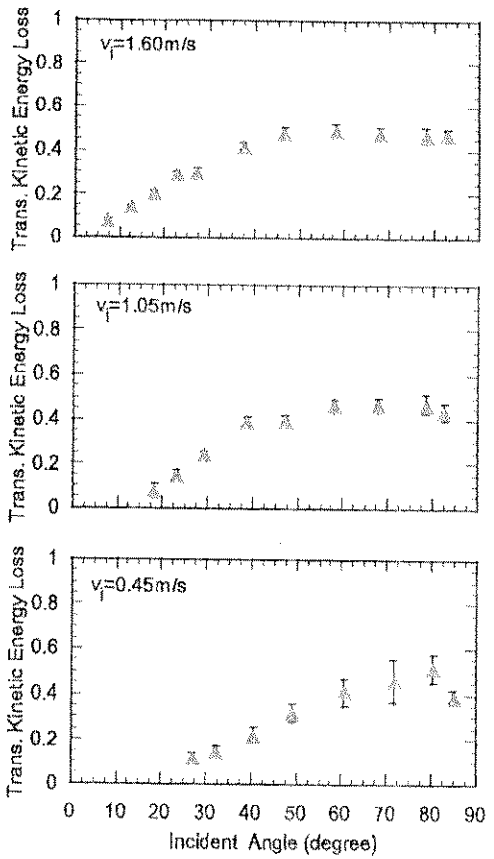

FIGURE 10 Comparison of the normalized energy loss, T_L, for stainless steel microspheres (SST65) with a molecularly-smooth, planar silicon crystal surface for 3 different ranges of total initial velocities; values indicated are nominal values.

where the microspheres are rolling without sliding on the surface at the end of contact. The observation was supported by the computational results of the rigid body model [5]. Starting from 50° down to 10°, the impulse ratio changes insignificantly and is basically constant ($\mu \approx 0.15$). This phenomenon was observed by Dunn *et al.* [5] and this region is designated as the "sliding region", where the microspheres are sliding (and rolling) on the surface at the end of contact. For this situation, a constant impulse ratio is interpreted as the sliding coefficient of friction according to the Amontons–Coulomb law.

For the $v = 1.05$ m/s and $v = 0.45$ m/s cases, the impulse ratio still increases when the incident angle decreases from 85° but the region of increasing impulse ratio becomes narrower. After that, the impulse ratio no longer is constant but decreases with decreasing incident angle. Some values even are less than or close to zero, which implies a zero-friction contact. The reason for the decreasing of impulse ratio with the decreasing of initial impact velocity is not clear yet. However, a dynamic simulation of the process reveals that these seemingly low impulse ratio values can be accounted for by assuming that the microspheres have a significant rotational velocity component prior to impact. The normalized translational kinetic energy loss is plotted in Figure 10. For the higher incident velocity case of $v = 1.60$ m/s, the loss is approximately constant from 85° down to 50°. From the energy loss equation, when the incident angle is large and μ is small, $T_L \approx (1 - e^2)$. Values of the coefficient of restitution change very slightly in this region so small differences should be expected in T_L. With the incident angles decreasing from 50°, the normalized energy loss decreases consistently to near zero. Based on rigid body mechanics, under an irrotational initial condition, η is equal to $\tan^{-1} \alpha_i$ where α_i is the incident angle. When the incident angle decreases, η^2 increases faster than η, and both are larger than unity for $\alpha_i < 45°$. Therefore, T_L almost always decreases for small incident angles. For $v = 1.05$ m/s, the constant normalized energy loss region becomes narrower (60° to 85°). This is even more apparent for the $v = 0.45$ m/s case in which the normalized energy loss decreases starting from 80°. In summary, the magnitudes of the incident velocities (translational and rotational) of the microspheres and the incident angle play a significant role on the particle's impact response.

2.4.3. Experimental Measurements of the Effect of Particle Shape

Most real microparticle impacts involve non-spherical particles. The effect of microparticle shape can be ascertained though comparison of spherical and non-spherical microparticles using the same substrate surface. To study the effects of microparticle surface roughness, *lycopodium* spores were used with molecularly-smooth silicon crystal substrate. *Lycopodium* spores are common bioaerosols. A surface

profile of a spore reveals that the surface is irregular and full of cavities. Comparisons of irregular particle surfaces (lycopodium spores, solid symbols) and smooth microsphere surfaces (stainless steel microspheres, SST76, open symbols) with a silicon substrate surface are shown in Figure 11. For the SST76, the coefficient of restitution is approximately constant from 90° down to 10°, where the value of e then decreases with decreasing incident angle. When the incident angle decreased from 90° to 55°, the magnitude of the coefficient of restitution in both cases is approximately the same, and the value is nearly constant. Both the material and the surface irregularity differences appear to have little effect on the impact response in this region. Below this region, the experimental results for these two cases show some differences. The coefficient of restitution for the *lycopodium* spores decreased from about 0.70 down to less than 0.55 when the incident angle decreased from 48° to 38°. Paw U [9] estimated that for 20–40 μm diameter *lycopodium* spores the capture velocity was 1.30 m/s when impacting American elm leaves. In the present experiments, the normal incoming velocity component ranged from about 1.10 m/s to 0.91 m/s for incident angles within 48° to 38°. Thus, based on this finding, one would expect to observe a decrease of the coefficient of restitution in this range that would continue as the incident angle is decreased further. However, for incident angles less than 38°, the coefficient of restitution for the *lycopodium* spores actually increases. This behavior has been observed before by Dunn *et al.* [5] with microspheres impacting a rough surface. Their analysis shows that surface roughness causes a fictitious increase in the measured value of the coefficient of restitution. The surface roughness of a *lycopodium* spore likewise may cause an increase of the coefficient of restitution as the incident angle is decreased. Other factors, such as multi-collisions and/or non-central collisions due to the irregular *lycopodium* spore surface can also contribute to this increase. No definite conclusions can be drawn.

The trends of the impulse ratio with changing incident angle also show the effect of microparticle surface geometry, friction and initial conditions. For the SST76 case, the impulse ratio increases consistently as the incident angles decrease from 90° down to about 50°. Then, it remains approximately constant from 50° to 10°. It increases again when the incident angles become smaller (below about 10°).

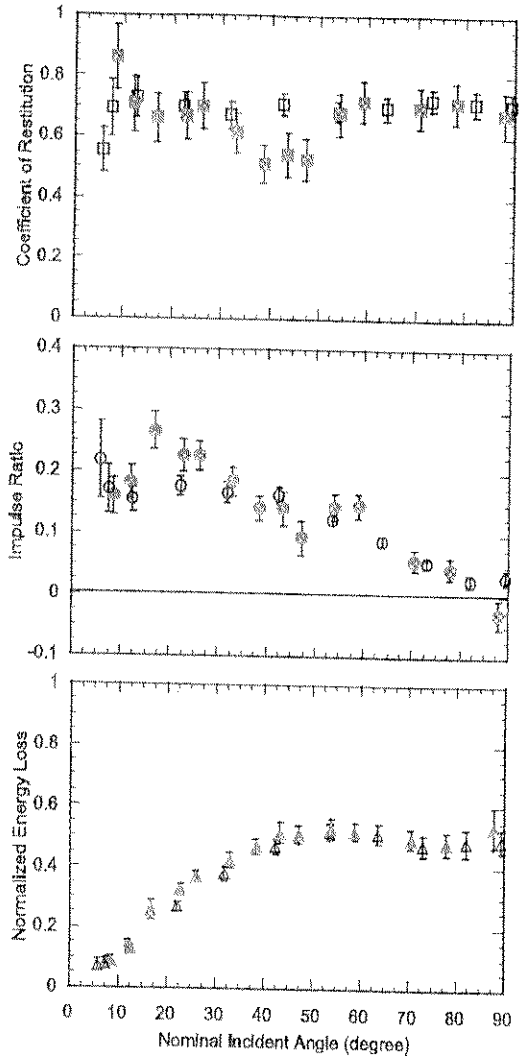

FIGURE 11 Comparisons of the impulse response from a silicon substrate surface of *lycopodium* spores (solid symbols) and stainless steel microspheres (SST76, open symbols).

As before, the increasing of the impulse ratio from 90° down to an incident angle of about 50° is explained by the microparticle rolling when it leaves the substrate surface at the end of contact. Below 50°, a constant impulse ratio occurs because of sliding throughout contact.

Below about 10°, the increase of the impulse ratio is suspected to be caused by adhesion. Adhesion increases the normal contact force and, therefore, the frictional force. The impulse ratio for the *lycopodium* spore behaves somewhat differently. There is no clear constant region. The impulse ratio increases as the incident angle decreases from 90° to about 20°. Then it decreases as the incident angle becomes less than 15°. The comparison of the normalized kinetic energy loss shows no substantial difference between these two cases. It seems that the differences in the microparticle and surface materials has no effect on the normalized kinetic energy loss under the present experimental conditions. From this observation, we learn that if we want to examine the effects of materials, surface geometry, *etc.*, on the impact response, the normalized energy loss, T_L, may not be the most sensitive parameter.

In summary, the microparticle's surface roughness complicates the behavior of e and μ. The coefficient of restitution at low incident angles exhibits trends similar to those observed for the rough substrate surface case, in which e rises with decreasing incident angle to values of unity or greater.

2.4.4. The Combined Effects of Particle Shape and Surface Roughness

Perhaps the most complex impact situation is that of a non-spherical microparticle contacting a typical rough indoor-room surface. Through comparison with the previously established base cases, these effects now are examined. Oblique impact experiments of *lycopodium* spores with a commercial *Formica* surface were conducted to explore the roughness effects of both substrate and particle. Profilometer scans of the *Formica* surface revealed an average surface roughness height of approximately 3.6 μm. The impact results are compared with those of SST76 microspheres impacting the same type of *Formica* surface and plotted in Figure 12. It can be seen that, for the same incident angles, the coefficient of restitution values for the stainless steel microsphere case (SST76, open squares) are significantly higher than those for the spore case (solid symbols), although the trends are similar. (Values of $e > 1$ occur as earlier in the rough-surface data in Figs. 6 and 7 and are explained in Section 4.) The coefficient of restitution increases with

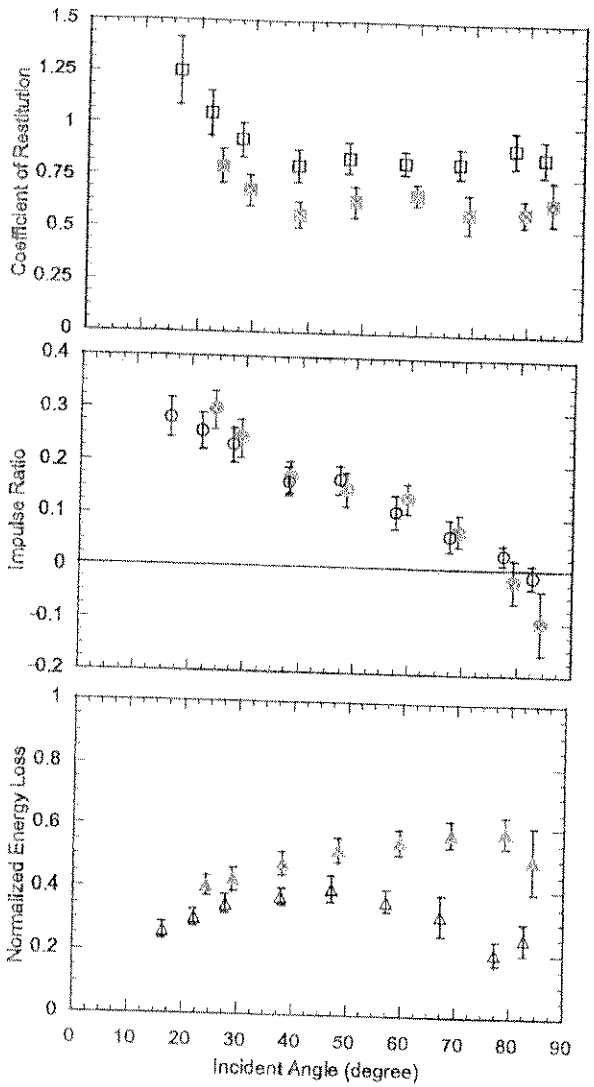

FIGURE 12 Comparisons of the impulse response from a commercial *Formica* surface of *lycopodium* spores (solid symbols) and stainless steel microspheres (SST76, open symbols).

decreasing incident angle for both cases. The measured values of the coefficient of restitution for the SST76 case exceed unity when the incident angle is less than 20°. This observation agrees with those

reported by Dunn *et al.* [5]. Differences between the *Formica* surface and the aforementioned silicon surface cause a remarkable difference in the coefficient of restitution. These may be explained by a conjunction of factors, such as the substrate and particle surface roughness and material properties. Under the present experimental set-up, only those events having both incident and rebound velocities were observed and analyzed. The observed increase of the coefficient of restitution at low incident angles does not necessarily mean that there was no capture in the experiments. A statistical analysis of *lycopodium* spore oblique impact onto surfaces is presented later and examines some of those effects.

The impulse ratio for these two cases is roughly the same. The surface roughness *of Formica* may be a dominant contributor to friction. If so, the difference of the microparticle surface geometry for a *lycopodium* spore and a SST76 microsphere is not very important, as far as the impulse ratio is concerned.

The normalized kinetic energy loss of the *lycopodium* spores onto *Formica* is higher, especially at higher incident angles. This is not surprising because it has already been seen that the *lycopodium* spores give a lower coefficient of restitution. For high incident angles, $T_L \approx (1 - e^2)$ and the normalized kinetic energy loss for *lycopodium* spores should be higher. For incident angles less than 45°, the difference of T_L between these two cases becomes smaller although the difference in the coefficient of restitution still is significant.

In summary, both particle and surface roughness significantly affect the impact process, the degree of which depends upon the specific materials involved. For low incident angles, both particle and surface roughness lead to apparent increases in the coefficient of restitution. The impulse ratio never achieves a constant value. Normalized translational kinetic energy losses are higher at high incident angles for the case of combined particle and surface roughness.

3. ANALYTICAL MODELS OF THE IMPACT PROCESS WITH ADHESION

The analytical models developed for the process of microparticle impact with a substrate surface are presented in this section. Each of

the analytical models is compared with the experimental results just presented.

The problem approached here is to investigate the impact mechanics of a microparticle just before, during and just after it collides with a surface in the presence of adhesion. The investigation specifically includes the effects of molecular attraction in the form of van der Waals force over the contact surface. Provisions were made to include other microforces [17], such as electrostatic and image forces; but this is not covered here. The problem includes determination of the rebound velocities of a microsphere that approaches a surface with arbitrary initial velocities (including angular velocities) and relating the impact process to the physical properties of the materials and to the adhesion force. The conditions under which the particle does not rebound (that is, it *attaches* or is *captured*) are of particular interest.

Two distinct but complementary models for the planar oblique impact of microspheres were developed. Both are derived directly from Newton's laws of motion. The first is an algebraic model based on the principles of rigid body impact and is referred to as the rigid body model. (The term *rigid body* refers not to a lack of flexibility of the microparticle, but rather that it is not treated as a point mass). The second is referred to as a dynamic simulation because it is based on the integration of ordinary differential equations of motion. Actually, there are two versions of the simulation. One is 2-dimensional or planar and the other is 3-dimensional. The two-dimensional simulation is described here; the three-dimensional dynamic simulation is an extension of the same concepts and will be described in a future technical paper. The rigid body model is algebraic and relatively simple. It imbeds the physical properties of the microsphere and surface (substrate) and impact process nonlinearities into 3 coefficients. A major difference between the models is that the rigid body model deals only in impulses and changes in momentum, whereas the simulation deals with displacements and forces. The simulation uses Hertzian theory to model the contact mechanics normal to the surface. It introduces a unique approach to modeling of the van der Waals force as a tensile ring force around the dynamic periphery of the compressive Hertzian contact area. Both models are *quasi-static* in the sense that they ignore wave motion

and model impact motion as a half-cycle of compressive vibration. Both models include tangential friction effects and can handle oblique impacts. The rigid body frictional model is completely general in the sense that tangential resistance to motion is from an impulse, without specifying the time-varying nature of the frictional force. The frictional force used in the dynamic simulation is more akin to Coulomb-type friction, but its formulation allows some versatility and permits changes as to how the friction force is developed. Both models have a common feature in that they distinguish between energy lost due to material deformation and energy lost in the adhesion process.

There are some basic, underlying assumptions to the dynamic simulation and rigid body model that deserve mention. The form taken by the simulation equations is a direct consequence not only of the assumptions mentioned above that energy dissipation due to adhesion and the particle-substrate materials are independent but, also, that plastic deformation plays an insignificant role in the dynamic contact process. The latter assumption is made due to the extremely short contact durations of microparticle impact and the consequent extremely high strain rates, in the order of 10^5 or higher. Current understanding is that plastic deformation develops through the process of dislocations and cannot develop at rates corresponding to such short time intervals. Moreover, objects whose dimensions are the order of magnitude of the microparticles are known to be less ductile and possess higher strength than like objects of much larger dimensions.

Studies were carried out related to the above models to augment or supplement their use. For example, a set of empirical equations was developed that can be used to represent the observed experimental behavior of the coefficient of restitution of the rigid body model for specific applications (specific materials, initial velocities, *etc.*). A unique feature of these equations is that the capture velocity can be determined from data taken near but not at capture conditions. Another auxiliary study is a Monte Carlo implementation of the rigid body model. This allows analysis of the impact process where one or more of the process parameters and/or initial conditions possess statistical variations. Another independent, but related, study that used the models is a sensitivity analysis of the impact process using

methods from the field of design of experiments. All of the above are described and summarized in the following.

3.1. Rigid Body Impact Model

The simpler of the two analytical models is an algebraic model based on Newton's laws in the form of impulse and momentum and follows from some of the work of Brach [15]. The model is remarkably simple yet surprisingly powerful. Figure 13 shows the basic geometry of a sphere in contact with a surface with a normal coordinate, n, positive away from the surface, and a tangential coordinate, t, along the surface. P_n and P_t are the normal and tangential components of the impulse over the full contact duration. A contact couple impulse, M, is illustrated but has been shown to be negligible by Brach *et al.* [16] and is omitted from the model. Notation is such that initial conditions (velocities, angles, *etc.*) are designated by lower case symbols and final conditions by upper case or capitals. A complete derivation of the model equations is given in Brach and Dunn [17]. A summary of the results is presented here. In addition to its simplicity, the model has two distinct applications to the study of microsphere impact. It can be used to analyze and interpret experimental data simply by plotting measured response data against the response predicted by the model. By using experimental data to represent the model's coefficients, the second use is as a predictive model for specific applications.

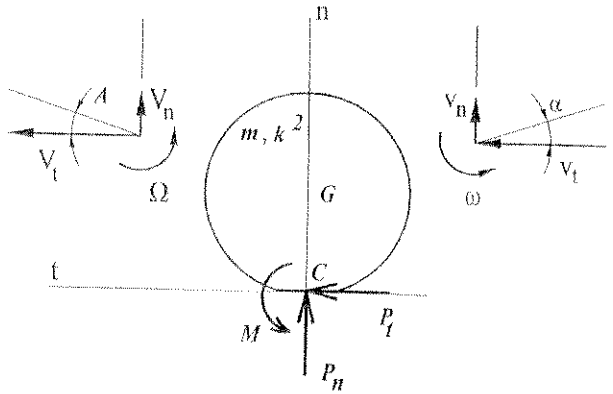

FIGURE 13 Free body diagram, variables and coordinates for the rigid body model of a microsphere impact.

3.1.1. Coefficients

Several coefficients are defined and used in the model. These are a coefficient of restitution in the absence of adhesion, R, an overall coefficient of restitution, e, an impulse ratio coefficient, μ, and an adhesion dissipation coefficient, ρ. The coefficient e is the commonly encountered kinematic coefficient of restitution defined as the ratio of the final to initial normal contact velocities as in Eq. (1). The impulse ratio is defined as the ratio of the tangential and normal components of the contact impulse (and leads to Eq. (2)):

$$\mu = P_t/P_n \tag{4}$$

The adhesion coefficient, ρ, is defined as the negative of the ratio of the (normal) impulse due to adhesion during rebound, P_A^R, to the (normal) impulse generated by deformation during approach, P_D^A, that is,

$$P_A^R = -\rho P_D^A \tag{5}$$

With the assumption that dissipation due to adhesion predominates during rebound, ρ gives a measure of the energy dissipation due to adhesion. The coefficients are not independent; e, R and ρ are related in a way that will be demonstrated in the next sections. The impulse ratio is related to the frictional drag that exists over the contact surface and is discussed shortly.

3.1.2. Solution Equations

The equations that provide the final conditions from known initial conditions are referred to as the solution equations. These are as follows.

$$V_n = -e\, v_n \tag{6}$$

$$V_t = v_t - \mu(1+e)\, v_n \tag{7}$$

$$\Omega = \omega + 5\mu(1+e)\, v_n/2\eta \tag{8}$$

$$P_D = -m(1+R)\, v_n \tag{9}$$

$$P_A^R = \rho R\, m v_n \tag{10}$$

Ω and ω are the final and initial angular velocities, respectively. An important auxiliary expression is for the tangential contact velocity, V_{Ct}, at point C. If this becomes zero at any time during the impact, the mode of motion of the sphere changes from sliding and rolling to rolling alone without sliding. This velocity is $V_{Ct} = V_t - r\Omega$ and can be expressed as

$$V_{Ct} = v_t - r\omega - 7\mu(1+e)/2\,v_n \tag{11}$$

The impulse ratio, μ_0, just large enough to cause rolling without sliding, or $V_{Ct} = 0$ is

$$\mu_0 = 2\eta/7(1+e) \tag{12}$$

where

$$\eta = (v_t - r\omega)/v_n \tag{13}$$

The impulse ratio represents tangential resistance to motion (frictional drag).

3.1.3. Energy Equations and Coefficients of Restitution, R and e

One of the most important aspects of a collision analysis is the energy loss. An expression for the energy lost during the collision can be found from the solution equations by subtracting the final kinetic energy from the initial using the solution equations to express final velocities in terms of the initial velocities and the coefficients. The energy loss, T_L, normalized to the initial translational kinetic energy, is:

$$2T_L/mv^2 = [(1-e^2) + 2\mu(1+e)\eta - \mu^2(1+e)^2]/(1+\eta^2), \tag{14}$$

Note that the value of impulse ratio, μ, is bounded by the level of friction in general, or friction coefficient when appropriate. For example, for a coefficient of friction f, $|\mu| \le f$. In general, the work of an impulse is given by,

$$W = \int F dx = \int F(\tau)\dot{x}d\tau = \int \nu(\tau)dp \tag{15}$$

Consider a normal impact. The gain of kinetic energy during rebound is $e^2(1/2mv_n^2)$. Using Eq. (15) the work of the normal impulse during rebound is $1/2R^2(1-\rho)mv_n^2$. Recall that R is the coefficient of restitution in the absence of adhesion. Similarly, the work, W_A, of P_A^R, the rebound adhesion impulse is $-1/2R^2\rho(1-\rho)mv_n^2$. Equating the kinetic energy gain to the work of the total rebound impulse gives the fundamental relationship

$$e^2 = R^2(1-\rho)^2 \tag{16}$$

Figure 14 is a schematic diagram showing the trends of the impact coefficients as the initial normal velocity changes. It shows that as the initial velocity gets smaller, if ρ reaches unity, e becomes 0. This occurs at the capture velocity, $v_n = v_c$, where the particle does not rebound.

For $\rho = 0$, the work of the body deformation impulse and the work (energy dissipated) of the adhesion impulse are R^2 and zero, respectively. For attachment, $\rho = 1$ and the rebound work term is zero. This gives $e^2 = 0$, as expected, but the works of the body and adhesion impulses should be equal and opposite, not zero. A more direct approach to work-energy can be developed. The energy loss in a collision can be written as the energy lost due to material dissipation, $(1-R^2)1/2mv_n^2$, and the energy lost due to the work done by

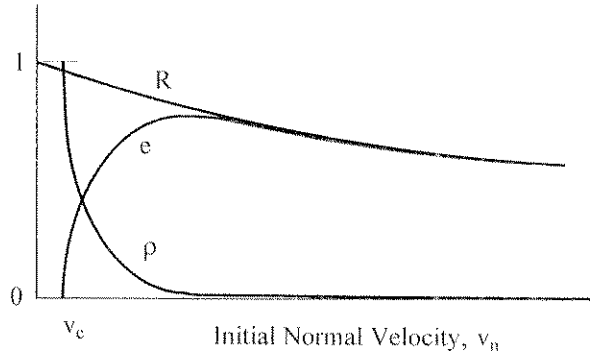

FIGURE 14 Trends of the restitution and adhesion coefficients for a microparticle impact.

adhesion, W_A. The total impact energy loss is:

$$T_L = (1 - e^2)1/2\,mv_n^2 = (1 - R^2)1/2\,mv_n^2 + W_A \tag{17}$$

The term including $1 - R^2$ is the energy lost due to dissipation in the sphere and W_A is the energy loss due to the work done by the adhesion force during rebound. Using Eqs. (16) and (17), the work done by the adhesion impulse (see Eqs. (5) and (10)) can be written as,

$$W_A = mv_n^2 R^2 \rho(2 - \rho)/z \tag{18}$$

For no adhesion, $\rho = 0$ and $W_A = 0$; for attachment (capture) $\rho = 1$ and the work of adhesion is $W_A = R^2\,mv_n^2/z$. Figures 15 and 16 show examples of the form of $e(v_n)$ for microsphere impact and illustrate the effects of adhesion on rebound as just discussed. The data in Figure 15 are direct experimental measurements [19] fit to empirical curves (discussed later) and the data in Figure 16 are from a dynamic impact simulation [25], similarly fit and described in the next section. Both illustrate the trend toward capture.

3.1.4. Impulse Ratio Coefficient, μ

Two distinct effects can be observed through examination of the impulse ratio. One is the effect of initial angular velocities and is most evident at high incident angles, near normal impact. The other is the

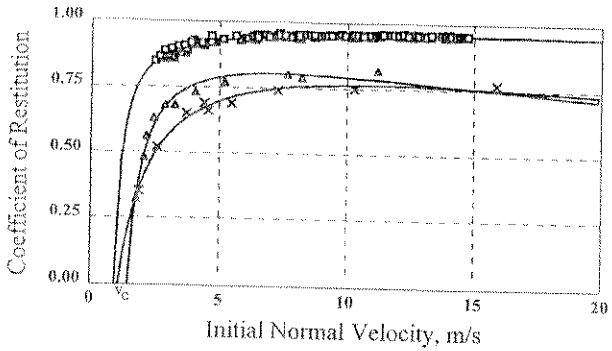

FIGURE 15 Experimental data from normal impacts: polystyrene latex particles on a quartz surface, □ ($v_c = 0.967$) [8]; ammonium fluorescein particles on molybdenum, Δ ($v_c = 1.47$), and mica, x ($v_c = 1.10$), surfaces [3].

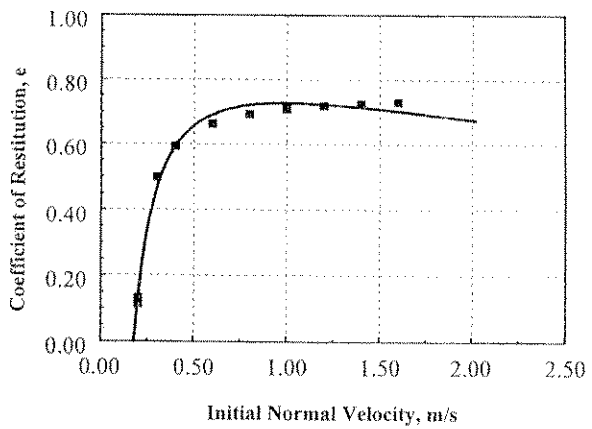

FIGURE 16 Simulation results based on experimental measurements, ■, of stainless steel microspheres impacting a silicon substrate, fit to the empirical equations; capture velocity is 0.18 m/s.

effect of adhesion causing a normal force and consequent frictional force for oblique collisions at very low initial normal velocities (low initial normal momentum).

All of the oblique impact experiments discussed here use the procedure where microspheres are dispensed vertically under gravity toward a target surface at a fixed distance from the dispenser. The surface is given a sequence of different orientation angles to produce different oblique angles of incidence, α. For a constant friction coefficient, f, and when the microspheres are not rotating as they fall ($\omega = 0$), the impulse ratio will follow the corresponding solid curves in Figure 17. For normal incidence, $\alpha = 90°$, and an initial angular velocity of $\omega = 0$, no tangential force and impulse will develop so $P_t = 0$, $\mu = 0$ and the result is the point $(\mu, \alpha) = (0, 90°)$. If $\omega \neq 0$, then $P_n \neq 0$ and then μ at 90° will be above or below the abscissa, depending on the sign of ω. Such effects of initial angular velocities were common; see Figures 6, 7, 11 and 12.

As α gets smaller the initial normal velocity component, the initial normal momentum and the normal impulse, P_n, approach zero and the consequent friction goes to zero. In the presence of adhesion, however, the normal force depends both upon the initial normal momentum and the adhesion force. As the angle of incidence grows small, adhesion pulls the particle toward the surface, creating an area

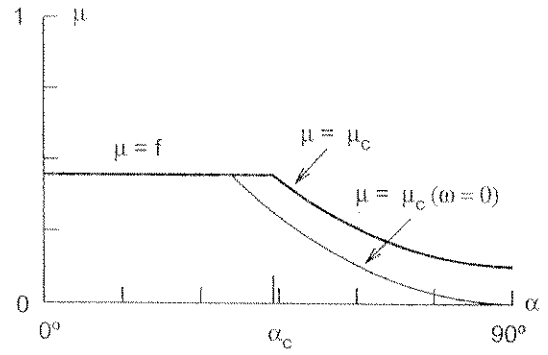

FIGURE 17 Idealized impulse ratio as a function of the angle of incidence for Coulomb friction as predicted by the rigid body model.

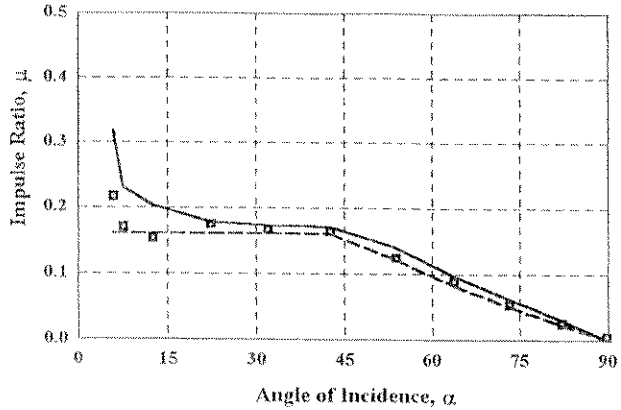

FIGURE 18 Impulse ratio as the angle of incidence changes for oblique collisions of stainless steel microspheres against a Si surface; dashed curve is from the rigid body model and the solid curve is from the simulation.

of normal compressive stress that supports friction. So, in the presence of adhesion, a frictional force and tangential impulse remain even as the initial normal momentum goes to zero. Consequently, the impulse ratio, $\mu = P_t / P_n$, grows as $\alpha \to 0$. This is reflected both in the experimental data and the simulation model and is shown in Figure 18. This upward trend of the impulse ratio has not been reported before. So, the rise in μ as $\alpha \to 0$ and $v_n \to 0$ for $v_t \neq 0$ is attributable to the presence and significance of adhesion.

3.2. Dynamic Simulation Model

A summary now is presented for the 2-dimensional simulation. A full derivation is contained in Brach and Dunn [17]. Figure 19 shows a free body diagram of a microsphere with an undeformed radius, r, whose mass center has elastic coordinates n and t and that rotates with angle θ with angular velocity $\omega = \dot{\theta}$. The normal displacement, n, of the mass center of a sphere is governed by Newton's second law. Combining Hertzian theory and the assumptions discussed above gives:

$$m\ddot{n} = \sqrt{r}K\, n^{3/2} - \sqrt{r}K\, n^{3/2}\, c_H\, \dot{n} - 2\pi a f_0 - 2\pi a f_0\, c_A\, \dot{n} \qquad (19)$$

Of the terms on the right hand side, the first is the classical Hertzian restoring force with stiffness parameter K. The second term is a dissipation term corresponding to the Hertzian force and represents dissipation in the materials. The third term represents idealized adhesion attraction as a conservative, circumferential (line) force. The last term adds dissipation due to adhesion. The quantities c_A and c_H are the damping coefficients for the adhesion and Hertzian damping, respectively. The terms in Eq. (19) that model the adhesion force and

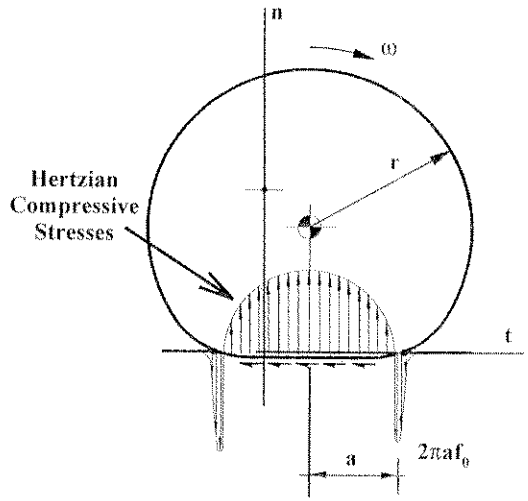

FIGURE 19 Idealized representation of the contact stresses showing the Hertzian compressive stress with a hemispherical distribution and adhesion represented as a ring stress around the periphery of the contact area.

dissipation may seem unorthodox. They specifically are chosen to provide a hysteretic form [17] for the adhesion force as is determined by measurement [23]. The contact radius, a, is related by Hertzian theory such that $a^2 = r\,n$. Hertzian stiffness, K, is given by:

$$K = 4/3\pi(k_1 + k_2)^2 \tag{20}$$

$$k_i = (1 - \nu_i^2)/\pi E_i \tag{21}$$

$$r = R_S r_S/(R_S + r_S) \tag{22}$$

Radii are the undeformed radius of the microsphere, R_S, and the local radius of curvature of the surface (substrate), r_S. For a flat surface, $r_S \to \infty$.

The damping terms can be modified by defining nondimensional dissipation parameters. The strength of the Hertzian dissipation rests in the magnitude of the constant c_H. A nondimensional parameter, ζ_H, is defined such that

$$\zeta_H = rc_H/T_H = c_H(R^3 K v_n^{1/2}/m)^{5/2} \tag{23}$$

where T is the period of contact predicted by Hertzian theory. Similarly, a nondimensional dissipation parameter is defined for the adhesion term as

$$\zeta_A = rc_A/T_H = c_A(R^3 K v_n^{1/2}/m)^{5/2} \tag{24}$$

For ζ_A and ζ_H to be constants it is necessary to use an appropriate nominal value of the initial normal velocity, v_n, for normalization; in fact, the capture velocity can be used, if known. Using these dissipation coefficients, the final form of Eq. (19) then becomes

$$\begin{aligned} m\ddot{n} = {} & \sqrt{r}K\,n^{3/2}\left[1 - \zeta_H(m/R^3 K v_n^{1/2})^{5/2}\,\dot{n}\right] \\ & - 2\pi\sqrt{rn}f_0\left[1 + \zeta_A(m/R^3 K v_n^{1/2})^{5/2}\,\dot{n}\right] = F_n(\tau) \end{aligned} \tag{25}$$

The model of the adhesion force used here is not derived from basic principles but rather represents an idealization of the force as observed over the past by others such as Johnson and Pollock [19], Fichman and Pnueli [20], Johnson *et al.* [21] and others, and as proposed by Brach and Dunn [17].

The tangential equation of motion is:

$$m\ddot{t} = F_t(\tau) \tag{26}$$

Tangential motion over the contact surface is considered to be either sliding or not sliding, so

$$F_t = -fF_n(\tau)\mathrm{sign}(\dot{t} - R\dot{\theta}),\ \dot{t} - R\dot{\theta} \neq 0 \tag{27}$$

where f is a frictional parameter (possibly a function) and

$$F_t = 0,\ \dot{t} - R\dot{\theta} = 0 \tag{28}$$

The third and final equation of motion governs angular motion and is:

$$I\ddot{\theta} = RF_t(\tau) \tag{29}$$

where I is the moment of inertia of the sphere.

3.2.1. Estimation of Dynamic Simulation Parameters

The parameters, or constants, that appear in the equations of the simulation model represent physical quantities such as mass and radius. Some of these are well known and are relatively easy to determine such as the Young's modulus, E, the coefficient of friction, f, and Poisson's ratio, ν. Other constants, such as the strength, f_0, of the adhesion ring force and damping, ζ_A, are not as easy to determine and could even be functions of v_n. Some of these are discussed in the following.

Assuming that f_0 remains relatively constant during an impact, its value can be estimated from equilibrium conditions. Using JKR theory, Li *et al.* [5] show that f_0 is related to the Dupré surface energy[4] constant, w_A, Hertzian radius, r, and stiffness, K, by

$$f_0 = (9Kr\,w_A^2/2\pi)^{1/3} \tag{30}$$

[4]The Dupré surface energy, w_A, has units of J/m^2 and actually is an energy density. In accordance with common usage, however, it will be referred to here as energy.

The procedure for determining the values of the two damping coefficients is through the use of experimental data taken at low and high initial normal velocities. For a high initial velocity (when adhesion dissipation is negligible), ζ_A is set to a value of zero and ζ_H is chosen by matching the experimentally-measured coefficient of restitution. With that value of ζ_H a value of ζ_A is then found by again matching the coefficient of restitution, but now at a low initial velocity. By repeating this process, a pair of nominal values of ζ_A and ζ_H is found that matches the coefficient of restitution over the desirable range of initial velocities and for specific materials. There seems to be very little information in the current literature concerning the mathematical nature of dissipation due to adhesion. For all of the simulation results, it is assumed that no significant adhesion dissipation occurs during establishment of adhesion, that is, during approach, so that $\zeta_A = 0$ for $\dot{n} < 0$. The simulation allows this to be changed if desirable.

The Hertzian stiffness, K, Eq. (20), is well defined for classical contact problems without adhesion. However, for the combined loading of inertial compression and adhesion, Hertzian theory must be augmented. The presence of adhesion makes a sphere deform somewhat more than in the absence of adhesion. This has been investigated by Brach *et al.* [22] and resulted in a reduced stiffness given by

$$K_R = K - \frac{5}{2}\left(\frac{5}{9}\right)^{5/2} \frac{w_A \pi R^2}{a_e^3} \tag{31}$$

where a_e is the static equilibrium value of the contact radius. The reduced stiffness should be used in place of K in applications of Eqs. (19) and (25).

3.2.2. Typical Results of the Dynamic Simulation

Some typical results are shown in Figure 20, taken from Li *et al.* [5]. This shows the normal contact force as it varies with time. These results are for the parameters of ammonium fluorescein spheres with a molybdenum substrate [3]. Compressive forces are shown as positive

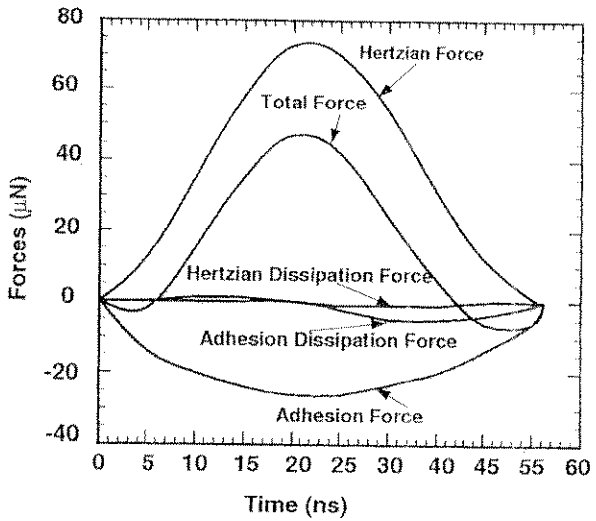

FIGURE 20 Typical simulation results showing the variations with time of the normal contact force. The case matches experimental results [3] for an ammonium fluorescein microsphere of diameter $d = 4.9\,\mu m$ impacting a molybdenum surface at 5.2 m/s. A value of $f_0 = 8.90$ N/m is used.

and the presence of adhesion is reflected by the negative dips to the total force near the beginning and end of contact. It is interesting to note that, for the conditions represented here, the dissipation forces are relatively small compared with the Hertzian and adhesion force.

Comparison of simulation results with experimental data are, of course, a major priority. This is not as easy at it sounds, however. The main reason is that while the simulation is capable of producing displacements, velocities, forces, *etc.*, as functions of time during contact, direct measurements of these quantities are virtually impossible for microparticles with present-day instrumentation and techniques. Only initial and final mass center velocities are measurable. This means that when parameters such as mass and radius are changed in the simulation, only their *effects* on rebound velocities and energy loss from observable data can be compared. Angular rotation and angular velocity of a microsphere, likewise, are impossible to measure. Such rotational velocities generally will exist due to the presence of frictional drag over the contact surfaces and may exist initially due to

prior impacts and during dispensing. Angular velocities and their changes are impossible to measure not only during contact but both before and after. Yet it is possible to assess the influence of angular velocities. For example, Dunn *et al.* [5] measured the approach and rebound velocities of stainless steel microspheres impacting a ultra flat silicon surface. The points in Figure 21 show kinetic energy loss based on the measured mass center velocities before and after impact. The two curves in the figure are from a corresponding simulation where the solid curve shows the true energy loss and the dashed curve shows the results of the dynamic simulation where the rotational kinetic energy has been ignored. Since the experimental data more closely match the dashed curve, it can be concluded that the rotational kinetic energy for microsphere impact can be significant. In fact, for an incident angle near 50° the final angular velocity from the simulation is about 2.3×10^4 rad/s. This should not be surprising since the final angular velocity, $\Omega = V_t / r$, where r is a radius of the order of 10×10^{-6} m. Another aspect of interest is the contact durations. Simulations of stainless steel microspheres and a silicon surface produce contact durations ranging from 300 to 700 ns. Based on half of this duration for approach and half for rebound, this implies strain rates as high as 10^5 to 10^6 s.

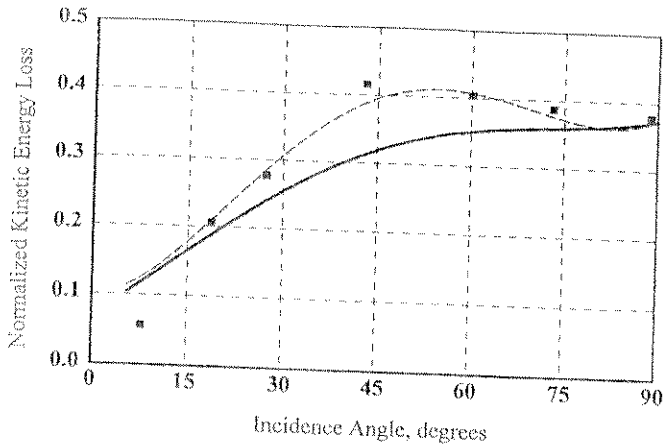

FIGURE 21 Points are experimental values of normalized kinetic energy loss for stainless steel microsphere impacts on a Si surface; solid and dashed curves are from the simulation where the dashed curved ignores energy due to the final angular velocity.

3.2.3. Applications of the Dynamic Simulation, Rolling Dissipation

One of the applications of the microsphere impact simulation was a study of the effects of rotational dissipation during contact. When rotation (rolling) of a microsphere takes place during contact and in the presence of adhesion, the leading edge of the contact area is continually establishing new contact with the surface and the trailing edge likewise is breaking contact (peeling). Since the adhesion process is not reversible, energy is lost. Consequently, rolling[5] in the presence of adhesion should cause a dissipation couple or moment over the contact area (see M in Fig. 13). A study was carried out by Brach *et al.* [16] that used the simulation and an independent mathematical analyses of the rolling contact problem to assess the effect of rotational dissipation. Their results show that the magnitude of rolling deformation and adhesion bond peeling couples are direct functions of the contact radius. Because the contact radius generally is relatively small, the effect of rolling dissipation can be neglected. This is why the moment impulse, M, in Figure 13 was neglected.

3.3. Empirical Equations

The rigid body model is based on the impulse and momentum equations of Newton's laws. The normal rebound of a microsphere is modeled simply as $V_n = -e\, v_n$, where the coefficient of restitution is treated as a constant in the collision problem. In actuality, e is a physical quantity that depends nonlinearly on the initial velocity, that is, $e = e(v_n)$. The other constants, R and ρ, also play a role as defined earlier. Actual behavior for specific materials, initial velocity ranges, *etc.*, is reflected in the model through $e(v_n)$. A series of empirical equations was suggested by Dunn *et al.* [4] and developed by Brach and Dunn [18] in which the constants are determined from data (experimental and/or analytical) through the use of fitting procedures.

[5]Note that rolling can occur simultaneously with sliding or in the absence of sliding. The latter is referred to as *pure rolling*.

A feature of these equations is that they can be used directly with the rigid body model and essentially tailor the model to specific applications. Another, and very important feature, is that they allow determination of the capture velocity using impact data from experiments where capture never actually occurs. In fact, it is difficult to measure directly the capture velocities since they represents a limiting behavior. When capture does occur, particles often collect on the surface and can hinder impact measurements.

The most convenient and effective form of the empirical equations is:

$$R = \frac{k_1^p}{k_2^p + |v_n|^p} \tag{32}$$

and

$$\rho = \frac{\kappa_1^q}{\kappa_2^q + |v_n - v_c|^q} \tag{33}$$

where the constants k, κ, p, q and v_c are determined from experimental data. All of these quantities have a functional dependence on the parameters of the impact and adhesion processes such as particle size, material properties, *etc.* Note that the k's and κ's have units of velocity.[6] For the simple case of $k_1 = k_2 = k$ and $\kappa_1 = \kappa_2 = \kappa$ and recognizing that $e = R(1 - \rho)$ from rigid body theory (see Eq. (16)), the overall coefficient of restitution becomes:

$$e = e(v_n) = \left[\frac{k^p}{k^p + |v_n|^p}\right]\left[1 - \frac{\kappa^q}{\kappa^q + |v_n - v_c|^q}\right] \tag{34}$$

These equations have been applied above, such as in Figures 15 and 16 in fitting of experimental and simulation data and for the determination of the capture velocity. Fitting of the equations and determination of the constants can be done in many ways, such as by least squares. Most data analysis software have such routines.

Combined with the empirical equations $e(R, \rho, v_n, v_c)$, the rigid body model is a versatile algebraic model of the impact process in

[6]Variations of these equations are possible and the equations can also be defined in terms of nondimensional velocities, v_n/k and/or v_n/κ.

the presence of adhesion. It first is used to study the effects of changes in the incident angle in order to study surface roughness. It then is used in a Monte Carlo analysis where the parameters are given statistical distributions. Examples of this are now discussed.

4. ANALYSES AND APPLICATIONS

4.1. Surface Roughness Effects

Consider a microsphere with a nominal angle of incidence, α, striking a surface with some waviness as shown in Figure 22. The microsphere strikes the surface at a point where the true normal is n' and the true angle is $\alpha+\phi$. The impact parameters, e and μ, characterize the mechanical processes normal and tangential to the true surface. However, their experimentally *measured* values are computed using velocity components measured relative to the nominal surface, that is, $e_m = -V_n / v_n$ and $\mu_m = (V_t - v_t)/(V_n - v_n)$. Expressions for the nominal velocity components, V_n, V_t, v_n and v_t, can be expressed in terms of the true velocity components, V_n', V_t', v_n' and v_t', using transformation equations. If this is done, the above two equations become, respectively,

$$e_m = \frac{e\cos\phi - V_t'\sin\phi/v_n'}{\cos\phi - v_t'\sin\phi/v_n'} \tag{35}$$

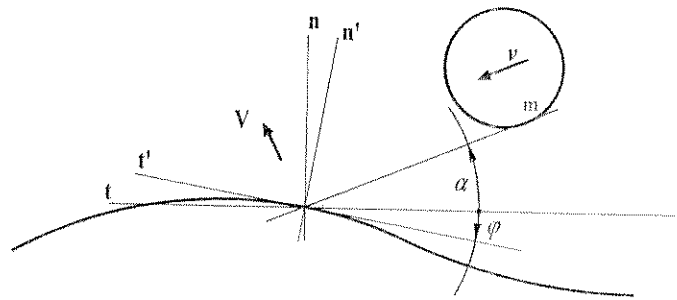

FIGURE 22 Apparent incidence angle, α, and normal coordinate, n, compared with true angle, $\alpha+\phi$, and normal coordinate, n', for variations in surface flatness.

and

$$\mu_m = \frac{\mu - \tan\phi}{1 + \mu\tan\phi} \tag{36}$$

where the subscript m denotes the measured values.

4.1.1. Shallow Angles of Incidence, $\alpha \approx 0$

It was noted earlier that for rough surfaces and shallow angles of incidence measured values of e exceed 1 (see Figs. 6, 7 and 12, for example). This can be explained using Eq. (35). Consider the case where both angles α and ϕ are small, such that $\cos\phi \approx 1$ and $\sin\phi \approx \phi$. Additionally, for a relatively low friction coefficient, f, sliding usually continues throughout the contact duration and $f\alpha \ll 1$. Under these conditions,

$$e_m \approx \left[1 + \frac{\phi}{\alpha}\right]\left[e + \frac{\phi}{\phi + \alpha}\right] \tag{37}$$

and

$$\mu_m \approx \mu - \phi, \quad \mu = \pm f \tag{38}$$

where $\tan\phi \approx \phi$ and $\mu\phi \ll 1$. The effect of waviness with a positive slope is to give a higher coefficient of restitution and give a negative bias to the impulse ratio. Note that for $\phi \approx \alpha$, e_m can exceed $2e$. So, although conservation of energy requires that $0 \le e \le 1$, measured values can exceed 1, or even 2.

4.1.2. Normal Incidence, $\alpha = \pi/2$

Normal incidence implies that $\alpha = \pi/2$ and $v_t = 0$. For normal and near normal impacts, rebound is under the condition of pure rolling, that is, $\mu = \mu_0$. However, if the microsphere has a high initial spin, or with any initial spin and low friction, it still will be sliding at separation. For a waviness with a small slope and the condition of rolling, the

experimental coefficient of restitution becomes:

$$e_m \approx e - \phi^2 + (1 + e)\,\mu_c\,\phi \tag{39}$$

The critical impulse ratio is:

$$\mu_0 = \frac{2}{7(1+e)}\frac{v_t' - r\omega}{v_n'} \tag{40}$$

When $\omega = 0$, $(1+e)\,\mu_c \approx -2\phi/7$ and $e_m \approx e - 9\phi^2/7$. When $\omega \neq 0$, a bias with the sign of ω can exist. For rolling at separation, the expression for the experimental value, μ_m, of the impulse ratio for normal incidence is

$$\mu_m \approx -\phi\left(1 - \frac{2/7}{1+e}\right) + \left(\frac{2/7}{1+e}\right)\frac{r\omega}{v_n'} \tag{41}$$

The angular velocity adds the potential for a bias to μ_m; otherwise, with $\omega = 0$, the measured impulse ratio is directly related to the slope, ϕ.

4.2. Monte Carlo Analysis

A computer program has been developed that allows various statistical distributions in arbitrary combinations to be assigned to process parameters. Written in the Microsoft Quick Basic language, the program permits a choice for each process parameter to be assigned a uniform, normal (Gaussian), standardized normal, lognormal or user-specified distribution. Random variables are generated through the use of the random number generator supplied with the Quick Basic language and the different distributions are generated through the use of the central limit theorem.

This program was applied to model the results of microsphere (SST76) impact with a rough surface (Formica). The actual microsphere diameter distribution (found to be normal) and the incident velocity distribution, both determined from direct measurements using the PDPA system, were inputs to the code. In addition, the empirically-determined local surface angle distribution (the distribution of ϕ) was another input. For each Monte Carlo calculation, a

randomly-selected value of ϕ was added to the incident angle, α, to yield the true surface angle, $\alpha+\phi$. Because there was no equivalent molecularly-smooth *Formica* surface available for comparison, it was assumed that such a surface behaved similarly to the molecularly-smooth silicon case. This required that the coefficient of restitution values needed to be adjusted to compensate for initial differences due to the different material properties of *Formica* and silicon. This was accomplished by simply subtracting from the coefficient of restitution values for each of the two cases the respective values at 85°; this is referred to as a relative coefficient of restitution.

The results of the Monte Carlo calculations are presented in Figure 23. The dashed line in the figure is a fit to the base case data

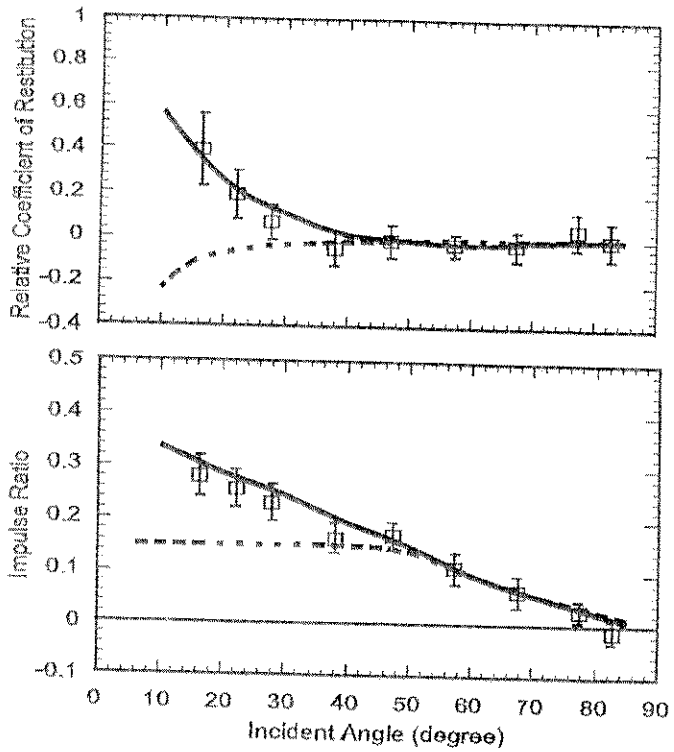

FIGURE 23 Monte Carlo method used with the rigid body model for a random variation in surface angle and particle diameter (solid curves) compared with experiments □ (with error bars) and deterministic rigid body results (dashed curves).

corresponding to the molecularly-smooth surface. The data are presented in the figure as open squares (see also Fig. 12) and the Monte Carlo results as solid lines. It is seen that the calculations follow the data very well. From approximately 90° down to 45°, the molecularly-smooth and rough surface cases are similar. Below 45°, they differ. As the incident angle is decreased, the relative coefficient of restitution for the rough surface increases toward unity, whereas, for the molecularly-smooth surface it decreases. Values of the impulse ratio for the rough case never become constant with decreasing incident angle, whereas, for the molecularly-smooth case, they become constant and equal to ≈ 0.15.

Thus, by considering the microparticle diameter and substrate local-incident-angle distributions, the Monte Carlo method can successfully predict the impact results of rough surfaces. This shows that the departure of experimental data from the ideal rigid body model can be attributed to surface roughness.

4.3. Sensitivity Analysis

The sensitivity of the impact process to variations in process parameters can be assessed using Monte Carlo techniques. However, other methods also are available. In particular, it is possible to use the methods of the design of experiments, DOE (see, for example, Guttman *et al.* [24]) to assess and rank which process parameters are the most significant. In particular, a study by Brach *et al.* [25] was carried out to determine which parameters are the most critical in influencing the capture velocity. The procedure used in the study contains the following steps:

1. define the dependent variable of interest, called the *response*, here the capture velocity,
2. define the parameters of interest, called *factors*,
3. establish nominal (typical) values of each factor as well as upper and lower *levels* of each factor,
4. determine the capture velocity for combinations of factors,
5. calculate the effect that each factor and factor interaction has on the response using DOE methods,
6. assess and rank the significance of the factors and their interactions.

The five factors chosen for this study are lettered A–E; they are: A, the Hertzian stiffness, K; B, the Dupré surface energy, w_A; C, microsphere radius, r; D, the damping constant, ζ_A, associated with adhesion energy dissipation and E, the damping constant, ζ_H, associated with material energy dissipation. Nominal values of the factors were chosen to correspond to stainless steel microspheres and the ultrasmooth silicon surface. These were chosen because of the availability of experimental data for these materials. The DOE method requires that each factor be assigned low and high values, (−/+). This was done in two different ways, resulting in two sets of results of the sensitivity study. The first set of upper and lower levels was treated as a process in estimating a realistic uncertainty in determination of the factors. The second procedure was simply to take ±5% of the nominal values for the upper and lower levels. Values of the capture velocity did not have to be determined for all possible

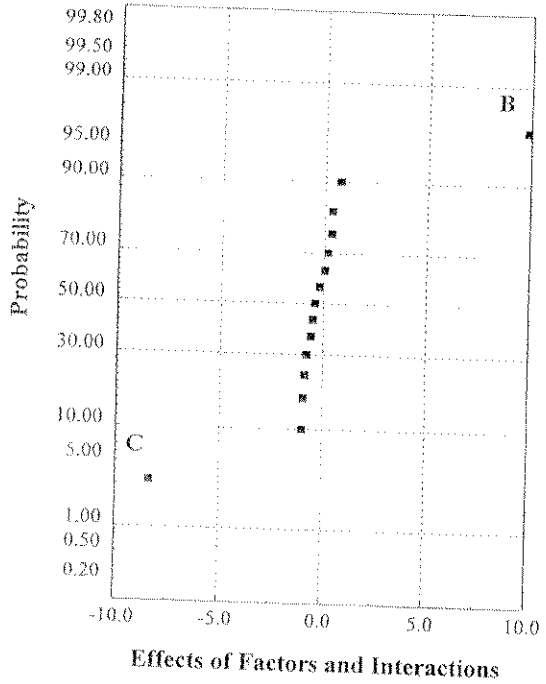

FIGURE 24 Effects of factors and factor interactions for *realistic* variations.

combinations of factor levels. This is possible through the use of a fractional factorial design.

The collision responses were calculated using the dynamic simulation model and the capture velocity values were found using the empirical fit equations. Figure 24 shows the results in the form of a normal probability plot of the effects and interactions from the analysis using levels based on factor uncertainty. It is quite clear that factors C, microsphere radius, and B, Dupré surface energy, stand out. This implies that these two variables control the capture process. The effect of radius is negative, indicating that the larger the radius, the lesser a tendency for capture conditions to exist and *vice versa*. The surface energy effect is positive, so the greater the Dupré surface energy, the more likely for capture to occur. The second part of the sensitivity study used *uniform* upper and lower levels and produced effects shown in Figure 25. Here, the influence of other factors begins

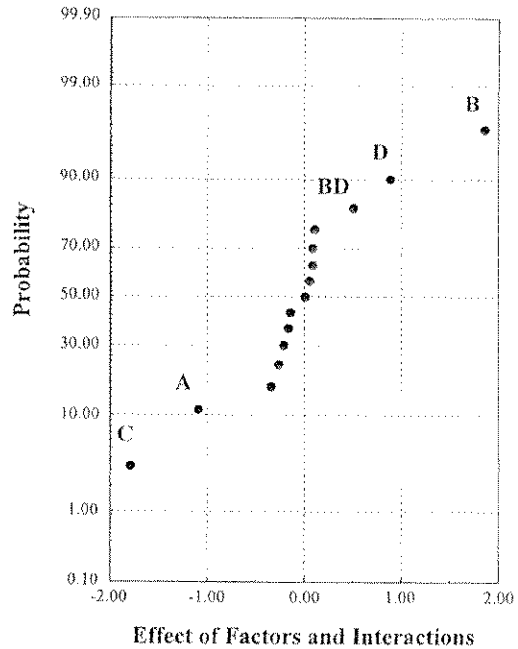

FIGURE 25 Effects of factors and factor interactions for *uniform* variations.

to appear. Again, factors C and B have the greatest influence, but factors A, Hertzian stiffness, and D, adhesion damping, show significance. The BD interaction, which is an interaction between Dupré surface energy and adhesion damping, also shows significance.

By and large, the results indicate that small particles with high adhesion energy are the most likely to be captured. Such a conclusion may seem to be rather obvious. Yet it does indicate that the other quantities such as the mechanical stiffness and material dissipation play secondary roles. Furthermore, such a conclusion also points out that the models being used (to generate the response values for the sensitivity analysis) agree with the intuition built up from observation of behavior of the impact-adhesion process. These results also agree with the observation made earlier of the relatively small magnitude of the dissipation forces from the simulation (see Fig. 20).

5. DISCUSSION

This section presents a discussion some of the more significant experimental and analytical results covered in this paper.

6. EXPERIMENTS

The experimental results reported herein are based on normal and oblique impacts of either microspheres and microparticles with either molecularly-smooth and rough surfaces. The experiments conducted using microspheres and molecularly-smooth surfaces served as an "ideal" base case with which other results were compared. All experiments were conducted in a vacuum chamber (see Fig. 1) and with charge-free surfaces and particles. Ideal, base-case conditions were chosen so that the van der Waals force acting at the contact surface was the only additional force due to the smaller size of the particle.

Normal impact experiments confirmed what others have found, that, as initial velocities decrease, there is a rapid decrease in the coefficient of restitution due to adhesion effects ending in capture at low velocities (for example, see Figs. 15 and 16). Capture velocities

decreased as particle size increased (see Fig. 4) because the effect of van der Waals force diminishes with increasing particle size.

Oblique impact experiments show that additional complexities occur when both friction and microsphere rotation are present. In the case of normal impacts, capture would usually manifest itself by a buildup of particles on the target surface. This did not happen for oblique impacts for two reasons. The first is because captured particles can roll away from the (tilted) target zone. But, perhaps more importantly, the conditions of capture for oblique impact were found to be different from that for normal impacts. Particles that were captured with a certain initial velocity during normal impacts were not captured with the same normal velocity (component) during oblique impacts. In fact, capture never was observed for oblique impacts (although this may have been because experimental initial velocities never were low enough). This was despite the fact that for oblique collisions friction combines with the van der Waals force to increase the impact energy loss. The presence of friction, however, does more than reduce the tangential velocity; it also causes a microsphere to take on a significant change in angular velocity. In fact, the final rotational velocities were determined to reach the order of 10^5 rad/s; kinetic energy associated with the (final) rotational velocity of the microspheres was found by modeling to be a significant portion of the overall final energy (see Fig. 21).

Collisions at small, or shallow, incident angles were found to be sensitive to surface roughness. When the approach angle was of the order of about 10° or less, surface roughness (variations in local surface slope) caused confounding of results. Under these conditions, coefficients of restitution calculated from experimental normal velocity measurements are significantly affected by differences between the actual, local normal direction and the target's nominal normal direction. Using the nominal instead of the actual normal angles in computation gave values of the coefficient of restitution greater than one (see Figs. 6 and 7, for example), a physical impossibility. This phenomenon was modeled analytically, verifying that roughness can lead to anomalous coefficient values if the actual normal surface direction is not used.

The effects of friction on impact were not measured directly because, depending on initial conditions (including initial angular velocities),

various combinations of sliding and rolling occur throughout the contact duration. Tangential effects were measured using the ratio of the change in tangential momentum to the change in normal momentum. This equals the ratio of the tangential to normal impulses, or the impulse ratio. Under a wide range of conditions, good agreement between the experimental impulse ratios and their theoretical counterparts from Coulomb's law was obtained (see Figs. 6b and 9a). This was not always the case, however (see Figs. 9b and 9c), especially when both rough surfaces and nonspherical particles were used.

7. MODELING

A significant departure was made in this research with respect to conventional assumptions of how energy is lost in the contact process. Many prior studies and models attribute the large majority of energy loss during microparticle impact to plastic deformation of the materials. Here, the view is taken that plastic deformation during impact is minimal, but that a significant amount of energy is lost due to the hysteretic nature of the adhesion process. The drop in the coefficient of restitution (as the initial velocity decreases) and capture, when it occurs (see Figs. 15 and 16), is attributed primarily to the effects of adhesion, not to plastic deformation.

Two analytical models of the impact process have been derived and applied extensively. One is a rigid body model (so named because it uses *rigid body* dynamics, not *point mass* dynamics). It is based on the principles of impulse and momentum and uses coefficients such as the coefficient of restitution, the impulse ratio and the adhesion coefficient. A fundamental assumption of the model is that the majority of contact energy loss (due to adhesion) occurs during rebound as opposed to approach. This allows the definition of an adhesion coefficient. In conjunction with the rigid body model, a set of empirical equations was developed that models the behavior of the impact coefficients as the initial velocity changes. The empirical equations are devised in such a way that they automatically determine a unique value of the capture velocity without direct measurements of the capture process itself (see Fig. 15).

A second analytical model simulates elastic behavior in the contact region using Hertzian theory and a new way of modeling the adhesion force, namely through the use of an attraction force with a ring geometry around the periphery of the contact region. Two distinct sources of dissipation are included, one related to strain and strain rate in the materials and the other due to adhesion dissipation. With the exception of the coefficients of these dissipation forces, all of the coefficients of the differential equation terms are determined directly from physical properties, including the adhesion force.

The dissipation coefficients were determined from experimental data for specific materials; this is because an analytical model for adhesion dissipation does not exist. For the sphere sizes and materials corresponding to the experiments, simulations showed that the peak adhesion force was approximately 1/3 of the peak Hertzian force and the corresponding peak adhesion dissipation force was about 1/5 of the peak adhesion force (see Fig. 20).

One of the primary uses of the rigid body model was to allow a comparison of the experimental values of the impact coefficients with impact behavior in the absence of adhesion. For example, the coefficient of restitution in the absence of adhesion typically approaches unity as the initial normal velocity approaches zero. In the presence of adhesion, however, the restitution coefficient approaches zero and the coefficient of adhesion approaches unity at the capture velocity. In general, for oblique impact and Coulomb's law of friction, the impulse ratio has a certain behavior as the angle of incidence changes (see Figs. 6 and 9); with some notable exceptions, this behavior was found applicable to microsphere impacts. An exception was for rough surfaces (see Fig. 12b) and some anomalous results for smooth surfaces (see Fig. 9). A Monte Carlo simulation, based on the rigid body model and using statistical distributions for the particle diameters, initial velocity and (rough) surface angles showed excellent agreement with corresponding data (see Fig. 23).

Finally, the simulation model was used to determine which physical parameters have the greatest influence on the capture velocity. Among the various physical parameters (such as Hertzian stiffness, adhesion dissipation, *etc.*) that influence the contact impact process, the microsphere radius and the Dupré surface energy were found to have the greatest influence on capture.

NOTATION

a	contact radius, m
e	impact coefficient; coefficient of restitution, velocities normal to the surface, rigid body model
c_A, c_H	coefficients of adhesion and Hertzian damping terms, simulation model, s/m
E	Young's modulus (modulus of elasticity), N/m^2
F	force, N
f	Coulomb friction coefficient
f_0	magnitude of adhesion ring force, simulation model, N/m
I	moment of inertia of sphere, m^2kg
K	Hertzian stiffness, N/m^2
k_i	empirical constant, empirical equations, m/s
K_R	reduced stiffness, N/m^2
m	mass, kg
P	Impulse, N-s
p	exponent, empirical equations
q	exponent, empirical equations
R	coefficient of restitution in the absence of adhesion, rigid body model
R_S	undeformed radius of microsphere, m
r	Hertzian radius of contacting bodies, m
r_S	radius of surface (substrate), m
T_H	period of Hertzian impact contact, s
T	kinetic energy, J
T_L	kinetic energy loss (initial minus final), J
V, v	final and initial velocity, respectively, rigid body impact model, m/s
w	Dupré surface energy constant (also, specific work of adhesion), J/m^2
W_A	work of the surface adhesion force (and impulse), J
$x, \dot{x}$	displacement, m, velocity, m/s
α	angle of incidence
η	ratio of initial tangential to normal contact point velocity, rigid body model
ϕ	angle
κ	empirical constant, empirical equations, m/s

μ	impact coefficient; ratio of normal and tangential impulse components, rigid body model
μ_0	critical impulse ratio; value of μ for zero final relative tangential contact velocity, rigid body model
ν	Poisson's ratio
Ω, ω	final and initial angular velocity, respectively, rigid body model
ρ	impact coefficient; ratio of adhesion impulse during rebound and elastic (deformation) impulse during approach
τ	time, simulation model, s
ζ_A, ζ_H	nondimensional coefficients of adhesion and Hertzian damping terms, simulation model

Subscripts

c	capture, empirical equations
m	measured, surface roughness analysis
n, t	normal, tangential components
e	equilibrium

Superscripts

A	approach phase of an impact, rigid body model
D	deformation
R	rebound phase of an impact, rigid body model

References

[1] Dahneke, B., "The Capture of Aerosol Particles by Surfaces", *J. Colloid Interface Sci.* **37**, 342–353 (1971).

[2] Wang, H. C. and John, W., "Dynamic Adhesion of Particles Impacting a Cylinder", In: *Particles on Surfaces, 1: Detection, Adhesion and Removal*, Mittal, K. L. Ed. (Plenum, New York, 1988), pp. 211–224.

[3] Wall, S., John, W., Wang, H.-C. and Goren, S. L., "Measurement of Kinetic Energy Loss for Particles Impact Surfaces", *Aerosol Science and Technology* **12**, 926–946 (1990).

[4] Dunn, P. F., Brach, R. M. and Caylor, M. J., "Experiments on the Low Velocity Impact of Microspheres with Planar Surfaces", *Aerosol Science and Technology* **23**, 80–95 (1995).

[5] Li, X., Dunn, P. F. and Brach, R. M., "Experimental and Numerical Studies on Microsphere Normal Impact with Surfaces", *J. Aerosol Sci.* **30**, 439–449 (1999).

[6] Caylor, M. J., "The Impact of Electrically Charged Microspheres with Planar Surfaces Under Vacuum Conditions", *Ph.D. Dissertation*, University of Notre Dame (1993).
[7] Dahneke, B., "Measurements of the Bouncing of Small Latex Spheres", *J. Colloid Interface Sci.* **45**, 584–590 (1973).
[8] Dahneke, B., "Further Measurements of the Bouncing of Small Latex Spheres", *J. Colloid Interface Sci.* **51**, 58–65 (1975).
[9] Paw U, K. T., "The Rebound of Particles from Natural Surfaces", *J. Colloid Interface Sci.* **93**, 442–452 (1983).
[10] Rogers, L. N. and Reed, J., "The Adhesion of Particles Undergoing an Elastic–Plastic Impact with a Surface", *J. Phys. D: Appl. Phys.* **17**, 677–689 (1984).
[11] Broom, G. P.,"Adhesion of Particles in Fibrous Air Filters", *Filtration and Separation* **16**, 661–669 (1979).
[12] Aylor, D. E. and Ferrandino, F. J., "Rebound of Pollen and Spores during Deposition on Cylinders by Inertial Impaction", *Atmos. Environ.* **19**, 803–806 (1985).
[13] Buttle, D. J., Martin, S. R. and Scruby, C. B., *Harwell Laboratory Report AERE-R13711*, Oxfordshire, UK (1989), pp. 1–30.
[14] Dunn, P. F., Brach, R. M. and Janson, G. G., "Surface Contact Mechanics during Oblique Impact of Microspheres with Planar Surfaces", *Aerosol Science and Technology* **25**, 445–465 (1996).
[15] Brach, R. M., *Mechanical Impact Dynamics* John Wiley, New York (1991).
[16] Brach, R. M., Dunn, P. F. and Cheng, W., "Rotational Dissipation During Microsphere Impact", *Aerosol Science* **10**, 1321–1329 (1999).
[17] Brach, R. M. and Dunn, P. F., "Macrodynamics of Microparticles", *Aerosol Science and Technology* **23**, 51–71 (1995).
[18] Brach, R. M. and Dunn, P. F., "Models for Rebound and Capture in Oblique Microparticle Impacts", *Aerosol Science and Technology* **29**, 379–388 (1998).
[19] Johnson, K. L. and Pollack, H. M., "The Role of Adhesion in the Impact of Elastic Spheres", *Midwest Mechanics Seminar Series*, University of Notre Dame (1993).
[20] Fichman, M. and Pnueli, D., "Sufficient Conditions for Small Particles to Hold Together Because of Adhesion Forces", *J. Applied Mech.* **52**, 105–108 (1985).
[21] Johnson, K. L., Kendall, K. and Roberts, A. D., "Surface energy and the contact of elastic solids", *Proc. R. Soc. Lond. A* **324**, 301–313 (1971).
[22] Brach, R. M., Li, X. and Dunn, P. F., "An Attachment Theory for Microsphere Adhesion", *J. Adhesion* **69**, 181–200 (1999).
[23] Horn, R. G., Israelachvili, J. N. and Pribac, F., "Measurement of the Deformation and Adhesion of Solids in Contact", *J. Colloid and Interface Sci.* **115**, 492 (1987).
[24] Guttman, I., Wilks, S. and Hunter, J., *Introductory Engineering Statistics*, 3rd edn. (John Wiley, New York, 1982).
[25] Brach, R. M., Li, X. and Dunn, P. F., "Parameter Sensitivity in Microsphere Impact and Capture", accepted for publication, *Aerosol Science and Technology* (1999).

The Adhesion of Irregularly-shaped 8 μm Diameter Particles to Substrates: The Contributions of Electrostatic and van der Waals Interactions

D. S. RIMAI

NexPress Solutions LLC., Rochester, NY 14653-6402, USA

D. J. QUESNEL

University of Rochester, Rochester, NY 14627-0132, USA

R. REIFENBERGER

Purdue University, West Lafayette, IN 47907, USA

The forces needed to remove irregularly-shaped, 8 μm diameter, polyester particles from a polyester substrate were measured using an ultracentrifuge. Measurements were also made on a second set of similar particles where nanometer-size silica clusters had been placed on their surfaces. These silica clusters acted as spacers, reducing direct contact between the particle and the substrate. It was found that the separation forces for the bare particles were consistent with predictions of the JKR theory of adhesion, but were much larger than could be accounted for from simple electrostatic interactions associated with either uniformly-charged particles or particles with localized charged patches. It was found, however, that the forces needed to effect separation decreased with increasing silica concentration. For particles with 2% by weight silica clusters on their surfaces, the separation force was only about 5% of the separation forces of the bare particles. At this concentration of silica, the estimates of the separation forces obtained from JKR theory, from the uniformly-charged model, and from the localized-charged-patch model are all about equal. The numerical estimates are consistent with the experimentally-obtained values.